NTNU – Trondheim
Norwegian University of
Science and Technology

Nanoflow of Protons and Water in Polymer Electrolyte Membranes

Bjørn Eirik Benjaminsen

Master of Science in Physics and Mathematics
Submission date: Januar 2013
Supervisor: Peter Berg, IFY

Norwegian University of Science and Technology
Department of Physics

Abstract

This master thesis studies the applicability of continuum mean-field theories such as the Poisson-Nernst-Planck equations and the Stokes equation. In particular, we investigate electro-osmotic flow of water and protons in infinite cylindrical nano-scale pores with a uniform surface charge density, representing pores in polymer electrolyte membranes. The impact of different modifications to the continuum theory is explored. Including finite-size ions in the Poisson-Boltzmann equation and spatially dependent profiles for permittivity and viscosity, values are found for the water drag coefficient and the pore conductivity. For surface charge densities $\sigma_s = -0.1$ to $\sigma_s = -0.5$ C m^{-2}, values of 2-5 are found for the water drag coefficient, compared to 7.5 to 22 for the unmodified equations. Similarly, values for the pore conductivity range from 5.5-30 S m^{-1} when including the modifications, compared to 13-100 S m^{-1} for the unmodified equations. A final modification to the Poisson-Boltzmann equations is made by including a field dependent explicit model for the permittivity. This model yields a permittivity profile comparable to predictions based on microscopic simulations, but with a lower permittivity near the wall. The proton concentration exhibits pronounced saturation effects near the wall.

Sammendrag

Denne masteroppgaven omhandler anvendelsen av kontinuum- og feltteorier som Poisson-Nernst-Plancks ligninger og Stokes ligning. Mer spesifikt, undersøkes elektro-osmotiske strømninger av vann og protoner i uendelige sylindriske nano-skala porer med en uniform overflateladningstetthet, som representerer porer i polymerelekrolyttmembraner. Virkningen av forskjellige modifikasjoner av kontinuumteorien undersøkes. Ved å inkludere ioner med endelig størrelse i Poisson-Boltzmann ligningen, samt romlig variable profiler for permittivitet og viskositet, finnes verdier for drag-koeffisienten til vannet samt konduktiviteten til poren. For overflateladningstettheter $\sigma_s = -0.1$ to $\sigma_s = -0.5$ C m^{-2} finnes verdier for drag-koeffisienten til vannet mellom 2 og 5, sammenlignet med mellom 7.5 og 22 for de umodifiserte ligningene. På samme vis finnes verdier for konduktiviteten til poren mellom 5.5 og 30 S m^{-1} når modifikasjonene inkluderes, sammenlignet med mellom 13 og 100 S m^{-1} for de umodifiserte ligningene. En siste modifikasjon av Poisson-Boltzmann ligningen blir gjort ved å inkludere en feltavhengig eksplisitt modell for permittiviteten. Denne modellen gir en permittivitetsprofil som kan sammenlignes med prediksjoner basert på mikroskopiske simuleringer, men med en lavere permittivitet nær veggen. Tettheten av protoner nær veggen viser tydelige metningseffekter.

Preface

This master thesis is the final step of the master program in Applied Physics and Mathematics at NTNU. The work was carried out in the autumn and winter of 2012-2013, from September to January. The thesis was written at the Department of Physics at NTNU under the supervision of Associate Prof. Peter Berg.

First and foremost, I would like to offer my sincerest thanks to my supervisor, Peter Berg, for his always valuable help and unwavering positivity and support. Furthermore, a thanks to Peder Aursand for help with LaTeX and to my girlfriend Trine and my family for supporting me all the way.

Contents

System Parameters and Variables,

a	Effective radius of H_3O^+
c	Concentration of protons
c_0	Proton concentration in pore center
k_b	Boltzmann constant
n_w	Number density or concentration of water
n_{w0}	Water concentration at center of pore
p_0	Magnitude of effective dipole moment of water
q	Proton charge
u	Fluid velocity
D	Diffusion coefficient of protons
E	Local electric field
E_{ext}	Applied electric field
F	Faraday constant
J_+	Proton flux
$\dot{M}$	Mass flux
P	Constant pressure gradient
R	Pore radius
R_C	Universal gas constant
T	Absolute temperature
ε	Relative permittivity of water

ε_0	Vacuum permittivty
ε_b	Bulk permittivity of water
ε_w	Permittivity of water near the wall
η_{drag}	Water drag
μ	Viscosity of water
μ_b	Bulk viscosity of water
μ_w	Viscosity of water near the wall
σ_p	Pore conductivity
σ_s	Surface charge denisity
ψ	Electric potential
ω	Molar weight of water

1 Introduction

The problem of flow of water and protons through nano-scale pores is complicated. Using mean-field and continuum equations such as the Poisson-Nernst-Planck (PNP) and Navier-Stokes equations to model the flow in such systems is problematic. There are significant wall effects for systems of this size, and one is close to the limit of applicability of the continuum approach. It is therefore of interest to study the applicability of the PNP and Navier-Stokes equations to such nano-scale systems. In particular, it is interesting to explore to what extent modifications made to existing continuum theory can yield more accurate results. This thesis will use a modified Poisson-Boltzmann (PB) equation [6, 10] with qualitative microscopic models for permittivity and viscosity to simulate electro-osmotic flow in nano-pores in non-equilibrium settings. A further modification to the Poisson-Boltzmann equation with an explicit model for the permittivity [22] will also be developed and studied. Few studies use modified PB equations in non-equilibrium settings [2]. Hence, this aims to be a worthwhile contribution.

Nano-pore systems are also interesting because of their similarity to the pores in polymer electrolyte membranes (PEM) used in PEM fuel cells. A short introduction to PEM fuel cells generally, and the PEM itself in particular, follows.

1.1 Polymer Electrolyte Membrane Fuel Cells

A polymer electrolyte membrane (PEM) fuel cell is an electrochemical energy conversion device. Because of its high energy density and excellent dynamic capability, it is the fuel cell of choice for application in transportation. It can also be used in portable and distributed/stationary power generation [50]. Key challenges of the PEM fuel cell technology include reliability and durability, efficiency, operation over large temperature ranges and, perhaps more importantly, its cost. The membranes used are expensive. In addition, platinum is used as a catalyst, and although the amount of platinum needed has dropped significantly in recent times [29], platinum is still a major contributor to the total cost of a PEM fuel cell.

The PEM fuel cell consists of a cathode and an anode separated by an electrolyte in the form of a thin polymer membrane. The membrane is an electronic insulator, but is a good conductor of protons [39]. At the anode, H_2 gas ionizes, splitting up into electrons (e^-) and protons (H^+) and releasing energy [29]

$$2H_2 \rightarrow 4H^+ + 4e^-. \tag{1.1}$$

The protons produced at the anode flow through the PEM to the cathode, where they react with oxygen and electrons. The latter are transported from the anode through an external circuit

$$O_2 + 4e^- + 4H^+ \rightarrow 2H_2O. \tag{1.2}$$

The reactions and charge flow are illustrated in figure 1.1

The overall reaction is then

$$O_2 + 2H_2 \rightarrow 2H_2O. \tag{1.3}$$

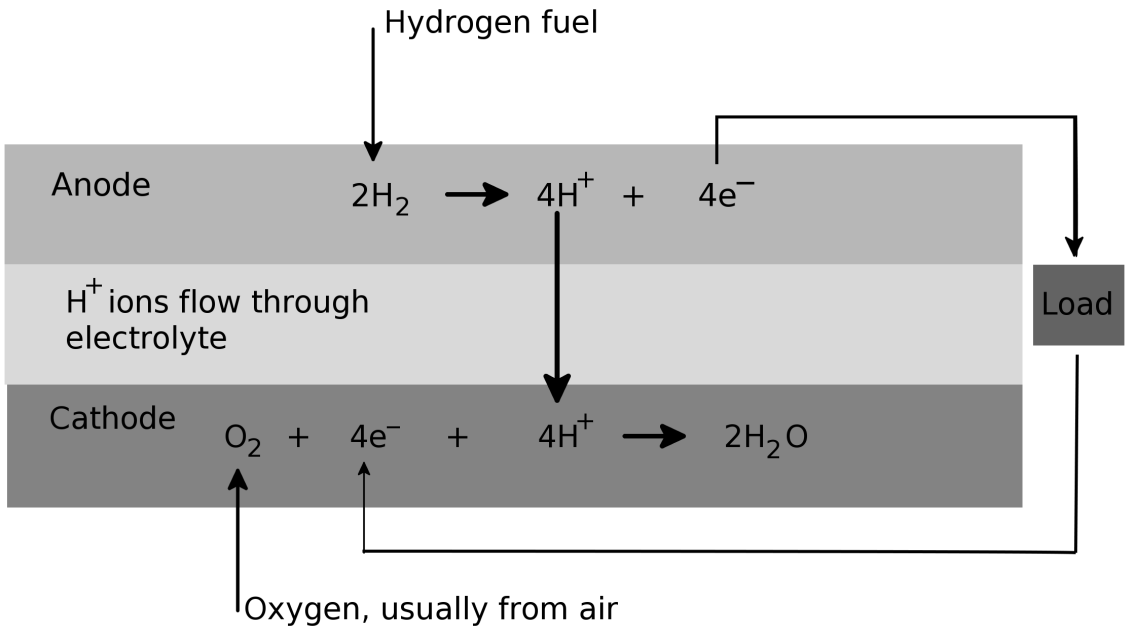

Figure 1.1: The half-cell reactions and charge flow in a PEM fuel cell

1.2 The Polymer Electrolyte Membrane

One main aspect of interest of a PEM in fuel cells is the conduction of protons, meaning its ability to transport protons from the anode to the cathode. The protons appear in the form of protonated water, so the PEM must be hydrated for it to allow the protons to move. The conductivity of protons increase more or less linearly with increasing hydration of the PEM. Nafion is the most common PEM for use in fuel cells, and there has been much research into the properties of Nafion membranes. The exact morphology is complex and not fully understood. One of the challenges is that it changes with the degree of water found in the membrane [30]. A short and somewhat

simplified overview of the morphology and properties of Nafion and similar PEMs follows.

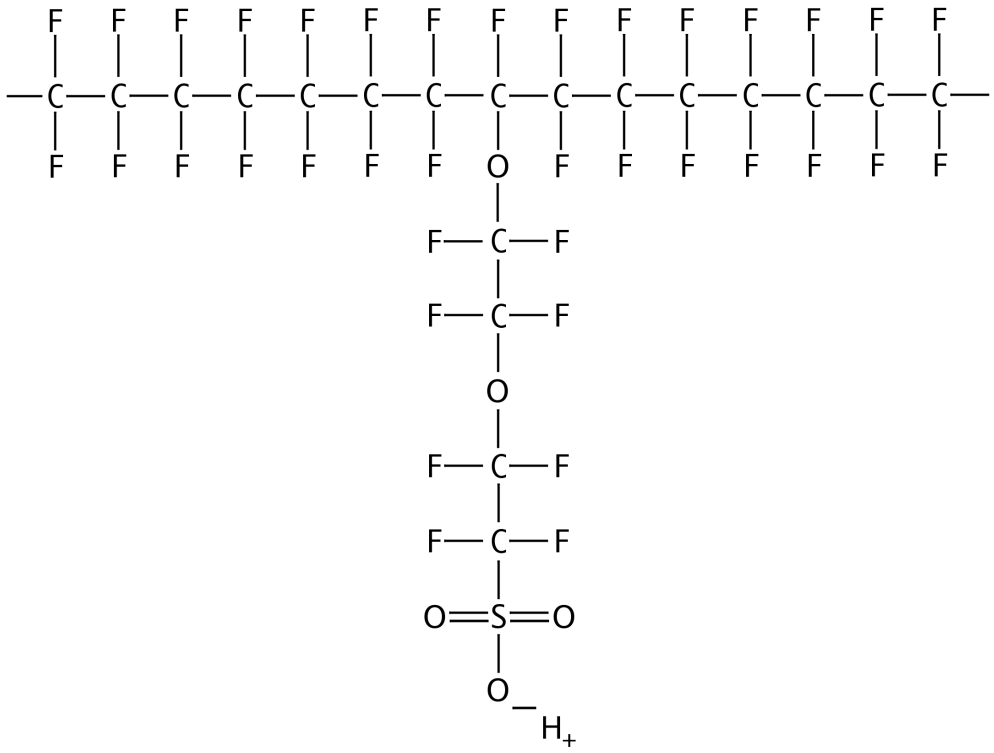

Figure 1.2: Example of the structure of sulphonated polytetrafluorethylene. The backbone is polytetrafluorethylene with an added side-chain ending in a SO_3H acid group.

The starting point is a hydrophobic backbone of polytetrafluorethylene. Side-chains are then added, each one ending in a sulfonic acid group (SO_3H) as shown in figure 1.2 The structure is called an ionomer, with the acidic SO_3H group being covalently bonded. This means the side chain actually ends in a SO_3^- ion under hydration [29]. The side chains tend to appear in clusters in the material [20]. The acid groups are highly hydrophilic, resulting in a phase-segregated medium with water-filled ionic clusters in an otherwise hydrophobic material. In one of the most referenced models by Gierke [19], clusters can be connected by narrow channels [23]. The hydration of the PEM is essential for its conduction of protons. As the water content of the PEM rises, the ionic clusters grow and create longer and wider pathways, enabling flow of water and protons [24, 47]. A more recent and simpler model for hydrated Nafion by Schmidt-Rohr and Chen [46] proposes that the PEM is made up of cylindrical nano-channels with a circular cross section with diameters between 1.8 and 3.5 nm, as illustrated in

figure 1.3. This model matches experimental data better than the Gierke model [12] and its geometry resembles that of the nano-pore model studied in this thesis.

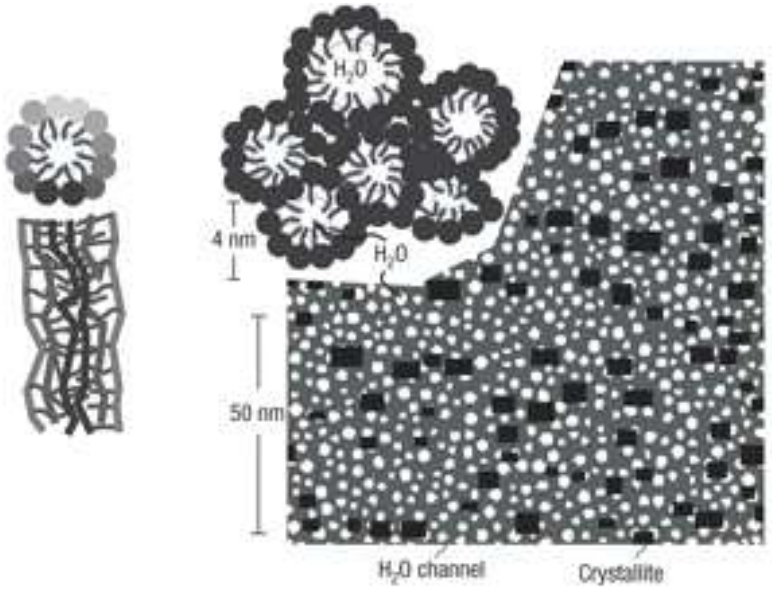

Figure 1.3: Structure of Nafion-like membranes. Long chain molecules with cylindrical water-filled hydrophilic regions containing clusters of sulphonated side-chains. The white areas are the water channels, while the gray and black are part of the Nafion membrane. Figure from Schmidt-Rohr and Chen [46].

When hydrated, the acid groups at the ends of the side chains enter into an ion exchange equilibrium with the nearby water and the dissolved mobile protons [5]. The protons form complexes with the water, and a simplified equilibrium can be written as

$$SO_3H + H_2O \leftrightharpoons SO_3^- + H_3O^+. \tag{1.4}$$

The simplification here is to consider only H_3O^+ complexes. In reality, the proton bonding in the water changes continuously and contains water complexes* larger than H_3O^+ [15].

The proton conductivity σ_p of the membrane is a measurable quantity. For well hydrated membranes, values of σ_p of around 0.06 S cm^{-1} have been found [35] . When protons move through the membrane, they drag water molecules along with them, increasing the flow of water from anode to cathode through the PEM. This electro-osmotic drag can cause the anode and parts of the membrane to dry out, which lowers proton conductivity considerably [14]. It is therefore an important effect in a PEM. The electro-osmotic or water drag coefficient, that is the number of water molecules

*In this thesis, we often refer to protons when we should say protonated water complexes

transported per proton, is measurable experimentally. Values of the water drag coefficient have been found to be around 1-3 [34, 51]. A third measurable effect is the water sorption of the PEM. It describes the water content of the PEM as a function of the relative humidity of the membrane environment. However, this will not be studied in this thesis.

1.3 Thesis Outline

This thesis is structured as follows. After this short introduction to the general subject, a description of the Poisson-Nernst-Planck and Stokes equations is included, along with a section about their applicability. This is kept brief, as the greater part of the work is computational in nature. Chapter 3 is more comprehensive, developing the models used in the simulations and providing additional theory where needed. Subsequently, the numerical method used for the simulations is described in chapter 4. Chapter 5 presents the plots produced in the simulations and discusses them in the context of existing literature. The last chapter offers a conclusion and an outlook for further research.

2 Poisson-Nernst-Planck Equations and Stokes Equation

2.1 The Continuum Approach to Electro-Osmotic Flow in Nano-Scale Channels

When dealing with electro-osmotic flow in nano-scale channels, a central question is to what degree continuum theory based on the Poisson-Nernst-Planck and Navier-Stokes equations can accurately describe the flow [25]. Some of the assumptions and simplifications are perhaps not valid when the number of molecules in the flow is very low. Ions are generally assumed to be point-like, all molecular interactions are treated with mean-field theory and properties such as the permittivity and viscosity are assumed to be constant.

An important concept in the electro-osmotic flow theory is the electric double layer. When a charged surface comes in contact with an electrolytic solution, counterions attract to the surface and build a layer of equal and opposite charge at the surface [41, 48]. The Stern model describes this layer as structured with a thin layer of ions tightly bound and immobile at the surface, often called the Stern layer, and a diffuse layer of mobile ions adjacent to it [1]. Figure 2.1 shows the structure of the double layer with an inner Stern layer and a diffuse layer.This diffuse layer is the main contributor to the electrokinetic effects, as the mobile ions can move under the influence of an electric field.

The area near the wall is the most important when dealing with electroosmosis. This is problematic, as it is near the wall that the atomistic effects are strongest. For example, the nature of the atomistic ordering near the wall can greatly affect the flow rate [48]. Microscopic models, such as molecular dynamics (MD) simulations based on interatomic potentials, can be used to study the flow more accurately, taking such wall effects into account [49]. However, MD simulations are computationally intensive and might therefore not always be practical. Another approach is to modify the continuum theory to incorporate microscopic models, or otherwise incorporate new physical properties. One such modification would be to somehow include finite-size ions. Such modifications have been proposed by, among others, Bikerman [6], Eigen [13] and more recently by Borukhov *et al.* [10, 11] and Bohinc *et al.* [8]. A similar modification is used in this thesis and will be introduced in more detail in the next

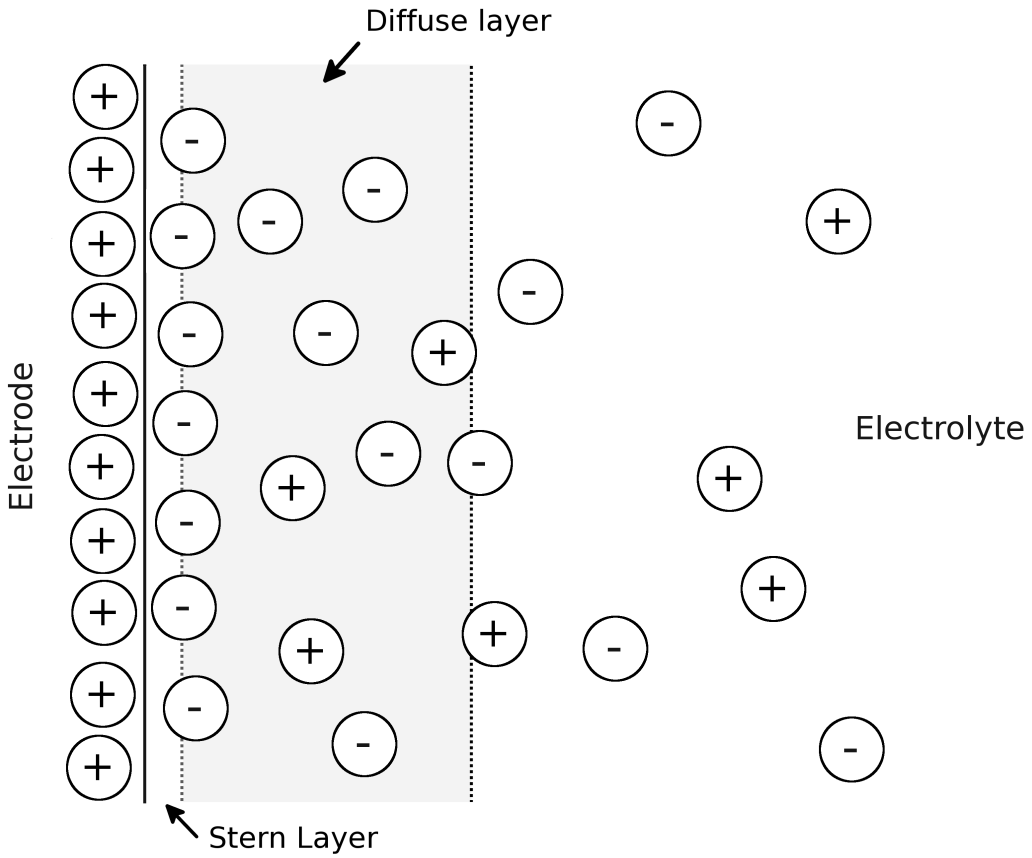

Figure 2.1: Structure of electric double layer in the Stern model. Ions in the inner layer are immobile [41].

chapter.

The value of the viscosity and permittivity in nano-channels is another topic of interest. Neither is found to be constant in nano-scale pores, deviating significantly from bulk values near the walls [2]. One way to incorporate this in a continuum model would be to use qualitative models based on results, for example, from MD simulations or experimental studies. The ideal approach would be to include models depending on the system parameters explicitly. An attempt at this is made in this thesis for the permittivity, by considering the ordering of water dipoles near the wall [22]. Wether an explicit model exists for the viscosity is still an open question.

The starting point for the continuum model of electro-osmotic flow will be the Poisson-Nernst-Plack equations coupled to Stokes flow. A short introduction will be given in the next section.

2.2 The Poisson-Nernst-Planck Equations

Consider a flow of water with a concentration c of protons and a velocity $\boldsymbol{u}$. In dilute solution theory, one usually writes the proton flux J_+ as [44]

$$J_+ = qc\boldsymbol{u} - D\left(q\nabla c + \frac{Fqc}{R_cT}\nabla\psi\right), \tag{2.1}$$

where q is the proton charge, D is the diffusion coefficient, ψ is the electrokinetic potential, T is the absolute temperature, and the constants F and R_c are the Faraday constant and universal gas constant, respectively. The first term in (2.1) is the convective flow. The second term is the electro-diffusion flux, which again has two terms. The first is a diffusional term proportional to the concentration gradient ∇c, which is essentially Fick's first law [7, 17]. The second is migrational and relates the electric force to a diffusive flux.

The electro-diffusion in (2.1) is governed by equations developed by Nernst and Planck [31, 32, 38]. The Nernst-Planck equation for the electro-diffusion describes charge conservation in the absence of sinks or sources and can in this case be written as

$$D\nabla\left(q\nabla c + \frac{Fqc}{R_cT}\nabla\psi\right) = 0. \tag{2.2}$$

Including the convective flow yields a new Nernst-Planck equation for convective electro-diffusion [45]

$$\nabla J_+ = \nabla\left(qc\boldsymbol{u} - qD\left(\nabla c + \frac{Fc}{R_cT}\nabla\psi\right)\right) = 0. \tag{2.3}$$

For the electric potential ψ, the Poisson equation holds

$$\Delta\psi = -\frac{qc}{\varepsilon\varepsilon_0}, \tag{2.4}$$

where Δ is the Laplace operator, ε is the relative permittivity, hereby referred to just as the permittivity, and ε_0 is the vacuum permittivity. We close the system of equations by imposing incompressibility

$$\nabla\boldsymbol{u} = 0. \tag{2.5}$$

Now, limiting the flow to an infinite, circular cylinder with a uniform surface charge density σ_s and a constant radius R, which is the system that is to be studied, we can write the full Poisson-Nernst-Planck equations from (2.3) and (2.4) as

$$\frac{1}{r}\frac{\mathrm{d}}{\mathrm{d}r}\left(r\frac{\mathrm{d}\psi}{\mathrm{d}r}\right) = -\frac{qc}{\varepsilon\varepsilon_0}, \tag{2.6}$$

$$\nabla J_+ = 0, \tag{2.7}$$

where the proton flux can be found from (2.1) as

$$J_+ = qu(r)c(r)\hat{e}_z - Dq\frac{\mathrm{d}c(r)}{\mathrm{d}r}\hat{e}_r + \frac{DFqc}{R_cT}\left(E_{\text{ext}}\hat{e}_z - \frac{\mathrm{d}\psi}{\mathrm{d}r}\hat{e}_r\right). \tag{2.8}$$

Here, $E_{\text{ext}} = -\frac{\mathrm{d}\psi}{\mathrm{d}z}$ can be interpreted as an external electric field.

Charge conservation and the symmetry of the pore ensures that the axial part of (2.8) is zero and that incompressibility is fulfilled, since $\boldsymbol{u} = u(r)\hat{e}_z$. The radial part of (2.8) must also be zero, as the cylinder is symmetric, infinite and of constant radius. Using this last fact, (2.6) and (2.8) can be combined to find the Poisson-Boltzmann (PB) equation [3]

$$\frac{1}{r}\frac{\mathrm{d}}{\mathrm{d}r}\left(r\frac{\mathrm{d}\psi}{\mathrm{d}r}\right) = -\frac{qc_0}{\varepsilon\varepsilon_0}\exp\left(-\frac{q\psi}{k_bT}\right), \tag{2.9}$$

where c_0 is the concentration of protons at the center of the cylinder and k_b is the Boltzmann constant. The distribution $c(r)$ of protons in the cylinder is then given by

$$c(r) = c_0\exp\left(-\frac{q\psi}{k_bT}\right). \tag{2.10}$$

2.3 Stokes equation

For an incompressible flow of water, driven by a constant pressure gradient ,$\nabla p = P$, and an external electric field E_{ext}, the Navier-Stokes equation can be written as [25]

$$\rho\left(\frac{\partial \boldsymbol{u}}{\partial t} + \boldsymbol{u}\cdot\nabla\boldsymbol{u}\right) = -P + \mu\Delta\boldsymbol{u} + qcE_{\text{ext}} \tag{2.11}$$

where $\boldsymbol{u}$ is the fluid velocity and μ is the viscosity. If the flow is at steady state and very slow, the Reynolds number is small and the entire left (inertial) part of (2.11) can be neglected, resulting in the Stokes equation. For the infinite, circular cylinder of radius R introduced in the previous section, the fluid velocity is purely axial so that $\boldsymbol{u} = u_z(r) = u(r)$, and we can write the Stokes equation as

$$0 = -P + \mu\frac{1}{r}\frac{\mathrm{d}}{\mathrm{d}r}\left(r\frac{\mathrm{d}u}{\mathrm{d}r}\right) + qc(r)E_{\text{ext}}. \tag{2.12}$$

Assuming no slip at the wall, the boundary conditions are

$$u(R) = 0 \tag{2.13}$$

and

$$\frac{\mathrm{d}u}{\mathrm{d}r} = 0 \quad \text{at} \quad r = 0 \tag{2.14}$$

where the second condition is a symmetry condition.

3 Model

Consider a cylindrical, circular pore with a uniform surface charge density σ_s, similar to Berg and Ladipo [4] and Berg and Findlay [3] (see figure 3.1). The pore has a radius R and is infinite in the z-direction. The flow through the pore is driven in the z-direction by an applied electric field E_{ext} and a constant pressure gradient P. This pore is similar to the cylindrical nano-channels in the model for hydrated Nafion proposed by Schmidt-Rohr and Chen [46]. The surface charge density σ_s relates to the ionic acid groups SO_3^- found in Nafion PEMs. In the ion exchange equilibrium in (1.4), some of the acid group side chains are charged, while others have a proton bound at the end. In this model, all the acid groups are assumed to be charged, i.e. all protons are dissociated. A concentration c of free protons inside the pore balances the surface charges on the pore walls.

We now need to look at how the protons are distributed inside the pore and how this affects the electrokinetic flow through the pore.

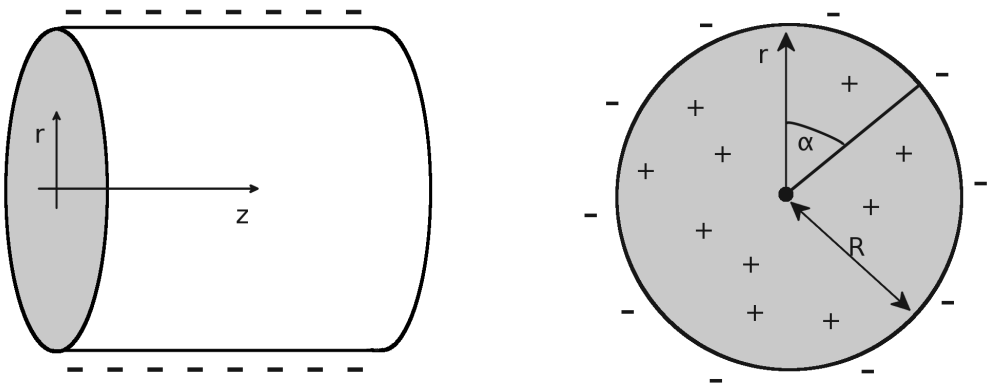

Figure 3.1: Pore geometry. To the left is an exterior view of the pore, to the right a cross section of radius R. The negative surface charges are uniformly distributed along the wall. Protons and water are present inside the pore.

3.1 Unmodified Poisson-Boltzmann Equation

From (2.9) we can write the Poisson-Boltzmann equation as

$$\frac{1}{r}\frac{\mathrm{d}}{\mathrm{d}r}\left(r\varepsilon(r)\frac{\mathrm{d}\psi}{\mathrm{d}r}\right) = \frac{qc_0}{\varepsilon_0}\exp\left(-\frac{q\psi}{k_bT}\right) \tag{3.1}$$

where $\varepsilon(r)$ is a spatially varying permittivity. The boundary conditions are then

$$\frac{\mathrm{d}\psi}{\mathrm{d}r} = 0 \quad \text{at} \quad r = 0 \tag{3.2}$$

and

$$\frac{\mathrm{d}\psi}{\mathrm{d}r} = -\frac{\sigma_s}{\varepsilon(R)\varepsilon_0} \quad \text{at} \quad r = R. \tag{3.3}$$

The first boundary condition is simply a symmetry condition. The second is a result of the global electro-neutrality of the pore. Following Berg and Findlay [3], the gauge

$$\psi(0) = 0, \tag{3.4}$$

is imposed on the system. Furthermore, the system is non-dimensionalized using the variable transformation $r = xR$, where x is a non-dimensional variable and R is the pore radius. Setting

$$\hat{\psi} = -\frac{q\psi}{k_bT}, \tag{3.5}$$

we can now write

$$\frac{1}{x}\frac{\mathrm{d}}{\mathrm{d}x}\left(x\varepsilon(x)\frac{\mathrm{d}\hat{\psi}}{\mathrm{d}x}\right) = \lambda e^{\hat{\psi}}, \tag{3.6}$$

where

$$\lambda = \frac{R^2q^2c_0}{\varepsilon_0k_bT}. \tag{3.7}$$

The new boundary conditions are then

$$\frac{\mathrm{d}\hat{\psi}}{\mathrm{d}x} = 0 \quad \text{at} \quad x = 0 \tag{3.8}$$

and

$$\frac{\mathrm{d}\hat{\psi}}{\mathrm{d}x} = -\frac{Rq\sigma_s}{\varepsilon(1)\varepsilon_0c_0k_bT} \qquad \text{at} \quad x = 1. \tag{3.9}$$

In addition, the condition (3.4) holds as

$$\hat{\psi}(0) = 0. \tag{3.10}$$

Differentiating (3.6) yields

$$\varepsilon(x)\frac{\mathrm{d}\hat{\psi}}{\mathrm{d}x} + x\frac{\mathrm{d}\varepsilon}{\mathrm{d}x}\frac{\mathrm{d}\hat{\psi}}{\mathrm{d}x} + x\varepsilon(x)\frac{\mathrm{d}^2\hat{\psi}}{\mathrm{d}x^2} = x\lambda e^{\hat{\psi}}. \tag{3.11}$$

Solving for the second derivative, we obtain

$$\frac{\mathrm{d}^2\hat{\psi}}{\mathrm{d}x^2} = \frac{\lambda e^{\hat{\psi}}}{\varepsilon(x)} - \frac{1}{x}\frac{\mathrm{d}\hat{\psi}}{\mathrm{d}x} - \frac{1}{\varepsilon(x)}\frac{\mathrm{d}\varepsilon}{\mathrm{d}x}\frac{\mathrm{d}\hat{\psi}}{\mathrm{d}x} \qquad (x \neq 0)\,, \tag{3.12}$$

which can be solved numerically with boundary conditions (3.8) - (3.10). Note that (3.6) with the conditions (3.8) - (3.10) poses a nonlinear eigenvalue problem, which has only a solution if the eigenvalue λ is chosen correctly.

Permittivity

The simplest model for the permittivity of the pore is a constant bulk value ε_b throughout the pore, as used by Berg and Ladipo [4] and Berg and Findlay [3]. This does not match MD results [27]. Near the wall the value for the permittivity is found to be significantly lower. This can be explained by the reduced ability of water dipoles near the SO_3^- groups to align with the electric field, thereby reducing polarization. Near the center of the pore, the permittivity reaches the bulk value for well hydrated pores, if the pore is not too small [27]. Paul and Paddison [37, 36] used a statistical mechanics model to produce a profile for the permittivity in a hydrated Nafion pore. Ladipo *et al.* [28] proposed an equation to fit that profile, given as

$$\varepsilon(r) = A + B\,\tanh\left(\frac{r - sR}{kR}\right), \tag{3.13}$$

where s and k are fit parameters, and A and B are constants given by

$$A = \varepsilon_b + \frac{(\varepsilon_w - \varepsilon_b)\tanh(s/k)}{\tanh(s/k) + \tanh((1-s)/k)} \tag{3.14}$$

and

$$B = \frac{(\varepsilon_w - \varepsilon_b)}{\tanh(s/k) + \tanh((1-s)/k)}. \tag{3.15}$$

Here, ε_w is the permittivity near the wall and ε_b is the bulk permittity. Figure 3.2 shows the profile for the permittivity in a 20Å pore.

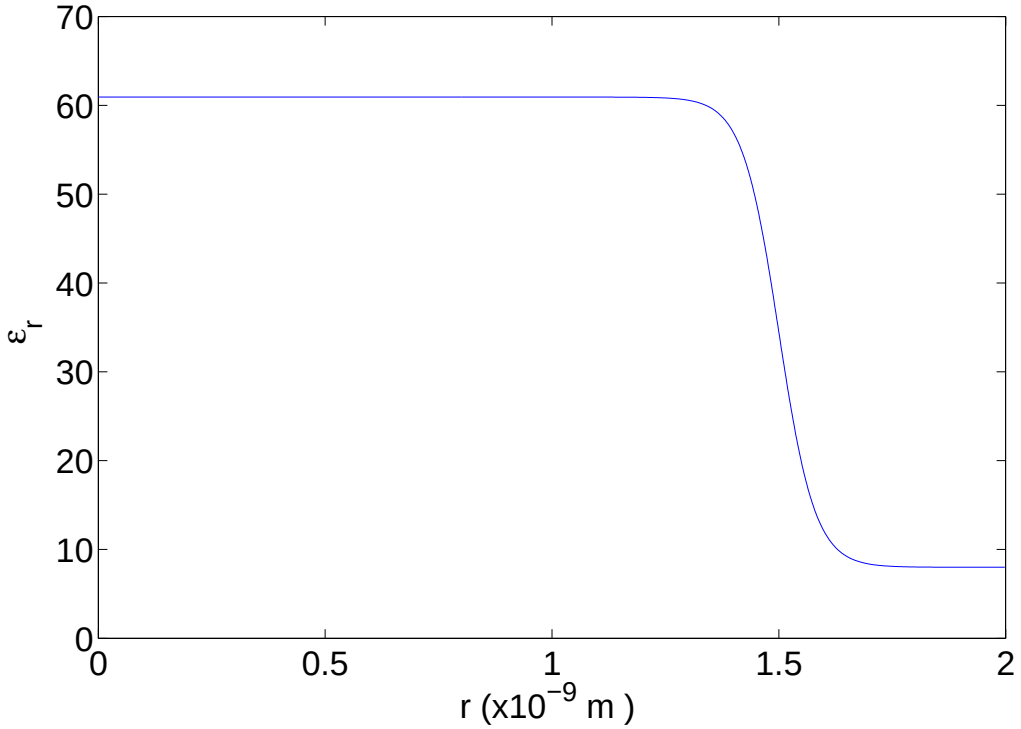

Figure 3.2: Profile of permittiviy in a $R = 20$Å pore. The value at the wall is $\varepsilon_w = 8$ [2], the bulk value at $T = 353$K is $\varepsilon_b = 60.93$. The fit parameters are $s = 0.5$ and $k = 0.08$.

3.2 Modified Possion-Boltzmann Equation

Treating the protons as point-like, as the unmodified Poisson-Boltzmann equation does, tends to give an exaggerated ion concentration near the wall, especially for large surface charge densities. There is nothing stopping the protons form occupying the same space, so the concentration could conceivably be several orders of magnitude larger than what is physically possible. One way of handling this is to introduce a finite size of the ions. This should limit the concentration at the wall and might introduce a Stern-layer like effect, depending on the size of the ions and the surface charge density [13].

Following Borukhov *et al.* [10, 11] an effective ion size a is introduced (we approximate the volume by a cube of length a). Now, the concentration of protons in the pore can be written as

$$c(x) = \frac{c_0 e^{\hat{\psi}}}{1 - a^3 c_0 + a^3 c_0 e^{\hat{\psi}}}. \tag{3.16}$$

This puts a limit on the maximum concentration which is now a^{-3}. Since we have chosen $\hat{\psi}(0) = 0$ in (3.10), the concentration at the center is still c_0. The main issue is then to choose the correct size for the protonated water complexes. This is not

straightforward, as the nature of the protons in water is complex. In this thesis, it will be assumed that the protons appear as H_3O^+ ions. The effective size is chosen to be $a = 2.2$ Å, slightly smaller than that of water (see further below). This is one of the criticisms of this model.

Introducing the new proton concentration into (3.6), we get

$$\frac{1}{x}\frac{\mathrm{d}}{\mathrm{d}x}\left(x\varepsilon(x)\frac{\mathrm{d}\hat{\psi}}{\mathrm{d}x}\right) = \frac{\lambda e^{\hat{\psi}}}{1 - a^3c_0 + a^3c_0e^{\hat{\psi}}} \tag{3.17}$$

with the same boundary conditions (3.8) - (3.10) as for the unmodified PB equation (3.6).

Differentiating and rearranging yields

$$\frac{\mathrm{d}^2\hat{\psi}}{\mathrm{d}x^2} = \frac{1}{\varepsilon(x)}\frac{\lambda e^{\hat{\psi}}}{1 - a^3c_0 + a^3c_0e^{\hat{\psi}}} - \frac{1}{x}\frac{\mathrm{d}\hat{\psi}}{\mathrm{d}x} - \frac{1}{\varepsilon(x)}\frac{\mathrm{d}\varepsilon}{\mathrm{d}x}\frac{\mathrm{d}\hat{\psi}}{\mathrm{d}x} \qquad (x \neq 0)\,, \tag{3.18}$$

which can be solved numerically.

3.3 Modified Poisson-Boltzmann Equation with Explicit Model for Permittivity

A different approach for finding the spatial variation of the permittivity is by considering the ordering of water dipoles within the local electric field E [21]. Permittivity models for point-like ions and small electric field strengths were presented by, among others, Onsager [33] and Kirkwood [26]. Generalized models have also been suggested [9]. Gongadze *et al.* [22] proposed a generalized model for point-like ions based on a modified Langevin PB equation. In that model, the water molecules are considered as Langevin dipoles and the number density of water is assumed to be constant, $n_w = n_{0w}$. An explicit form of the effective permittivity of the electrolyte is found as

$$\varepsilon_{\text{eff}} = 1 + n_{0w}\frac{p_0}{\varepsilon_0}\frac{L(p_0E/k_bT)}{E}, \tag{3.19}$$

where p_0 is the magnitude of the water dipole moment and $E = -\frac{\mathrm{d}\psi}{\mathrm{d}x}$ is the local electric field. The function $L(U)$ is the Langevin function given by

$$L(U) = \coth(U) - \frac{1}{U}. \tag{3.20}$$

In (3.19), the Langevin function effectively gives the average magnitude of the Langevin dipole moments at that point in the pore.

The assumption that the number density of water is constant throughout the pore does not hold when the ions present in the water are protons, unless the number of protons $c(x)$ is very low compared to n_{w0}. The protons bond with the water and form H_3O^+ ions, or larger complexes [15]. Near the walls, $c(x)$ increases dramatically, and so a constant n_w is unrealistic. Using the hydronium distribution $c(x)$, a spatially varying number density $n_w\left(\hat{\psi}(x)\right)$ can be written as

$$n_w\left(\hat{\psi}(x)\right) = n_{0w} - c\left(\hat{\psi}(x)\right) = n_{0w} - \frac{c_0 e^{\hat{\psi}(x)}}{1 - a^3 c_0 + a^3 c_0 e^{\hat{\psi}(x)}} \tag{3.21}$$

and thereby a new equation for the permittivity as

$$\varepsilon_{\text{eff}} = 1 + n_w(\psi)\frac{p_0}{\varepsilon_0}\frac{L(p_0 E/k_b T)}{E}. \tag{3.22}$$

Strictly speaking, we should write $n_w a_w^3 + c a^3 = 1$ which is approximated by (3.21) in the case of $a_w \approx a$, where a_w is the size of the water molecule.

A new modified PB equation can now be written, using the finite-size ion concentration (3.16) and the permittivity (3.22) as

$$\frac{1}{x}\frac{\mathrm{d}}{\mathrm{d}x}\left(x\varepsilon(\hat{\psi}, E)\frac{\mathrm{d}\hat{\psi}}{\mathrm{d}x}\right) = \frac{\lambda e^{\hat{\psi}}}{1 - a^3 c_0 + a^3 c_0 e^{\hat{\psi}}}, \tag{3.23}$$

where $\varepsilon(\hat{\psi}, E) = \varepsilon_{\text{eff}}$. The boundary conditions (3.8)-(3.10) are still valid. The differentiation yields

$$\varepsilon(\hat{\psi}, E)\frac{\mathrm{d}\hat{\psi}}{\mathrm{d}x} + x\left(\frac{\partial\varepsilon}{\partial\hat{\psi}}\frac{\mathrm{d}\hat{\psi}}{\mathrm{d}x} - \frac{k_b T}{q}\frac{\partial\varepsilon}{\partial E}\frac{\mathrm{d}^2\hat{\psi}}{\mathrm{d}x^2}\right)\frac{\mathrm{d}\hat{\psi}}{\mathrm{d}x} + x\varepsilon(\hat{\psi}, E)\frac{\mathrm{d}^2\hat{\psi}}{\mathrm{d}x^2} = \frac{x\lambda e^{\hat{\psi}}}{1 - a^3 c_0 + a^3 c_0 e^{\hat{\psi}}}. \tag{3.24}$$

Here, we have from (3.22)

$$\frac{\partial\varepsilon}{\partial E} = \frac{\partial}{\partial E}\left[1 + n_w(\psi)\frac{p_0}{\varepsilon_0}\frac{L(p_0 E/k_b T)}{E}\right]. \tag{3.25}$$

Substituting $U = p_0 E/k_b T$ and differentiating gives

$$\frac{\partial\varepsilon}{\partial U} = \frac{\partial}{\partial U}\left[1 + n_w(\psi)\frac{p_0^2}{\varepsilon_0 k_b T}\frac{L(U)}{U}\right] = n_w(\psi)\frac{p_0^2}{\varepsilon_0 k_b T}\frac{L'(U)U - L(U)}{U^2} \tag{3.26}$$

where

$$L'(U) = \frac{\mathrm{d}L}{\mathrm{d}U} = 1 - \coth^2(U) + \frac{1}{U^2} \tag{3.27}$$

so that

$$\frac{\partial\varepsilon}{\partial E} = \frac{\partial\varepsilon}{\partial U}\frac{\mathrm{d}U}{\mathrm{d}E} = n_w(\hat{\psi})\frac{p_0^3}{\varepsilon_0 (k_b T)^2}\frac{U + \frac{2}{U} - \coth^2(U) - \coth(U)}{U^2}. \tag{3.28}$$

Furthermore, we can write

$$\frac{\mathrm{d}\varepsilon}{\mathrm{d}\hat{\psi}} = \frac{\mathrm{d}}{\mathrm{d}\hat{\psi}}\left[1 + n_w(\hat{\psi})\frac{p_0}{\varepsilon_0}\frac{L(p_0E/k_bT)}{E}\right] = \frac{\mathrm{d}n_w}{\mathrm{d}\hat{\psi}}\frac{p_0}{\varepsilon_0}\frac{L(p_0E/k_bT)}{E} \tag{3.29}$$

where

$$\frac{\mathrm{d}n_w}{\mathrm{d}\hat{\psi}} = \frac{\mathrm{d}}{\mathrm{d}\hat{\psi}}\left[n_{0w} - \frac{c_0e^{\hat{\psi}(x)}}{1 - a^3c_0 + a^3c_0e^{\hat{\psi}(x)}}\right] = -\frac{c_0e^{\hat{\psi}}(1 - a^3c_0)}{\left[1 - a^3c_0 + a^3c_0e^{\hat{\psi}}\right]^2} \tag{3.30}$$

so that

$$\frac{\partial\varepsilon}{\partial\hat{\psi}} = -\frac{c_0e^{\hat{\psi}}(1 - a^3c_0)}{\left[1 - a^3c_0 + a^3c_0e^{\hat{\psi}}\right]^2}\frac{p_0}{\varepsilon_0}\frac{L(p_0E/k_bT)}{E}. \tag{3.31}$$

Rearranging (3.24) now yields

$$\frac{\mathrm{d}^2\hat{\psi}}{\mathrm{d}x^2} = \frac{\dfrac{\lambda e^{\hat{\psi}}}{1 - a^3c_0 + a^3c_0e^{\hat{\psi}}} - \dfrac{1}{x}\varepsilon(\hat{\psi}, E)\dfrac{\mathrm{d}\hat{\psi}}{\mathrm{d}x} - \dfrac{\partial\varepsilon}{\partial\hat{\psi}}\left(\dfrac{\mathrm{d}\hat{\psi}}{\mathrm{d}x}\right)^2}{\varepsilon(\hat{\psi}, E) - \dfrac{k_bT}{q}\dfrac{\partial\varepsilon}{\partial E}\dfrac{\mathrm{d}\hat{\psi}}{\mathrm{d}x}} \tag{3.32}$$

which can be solved numerically using (3.28) and (3.31). This is now a very complicated non-linear eigenvalue problem.

3.4 Stokes equation

Rewriting the Stokes equation (2.12) with the non-dimensional variable x and rearranging yields

$$\frac{\mathrm{d}}{\mathrm{d}x}\left(\mu(x)x\frac{\mathrm{d}u}{\mathrm{d}x}\right) = PR^2x - qc(x)ER^2x. \tag{3.33}$$

The expression $\mu(x)$ is here a spatially varying viscosity and $c(x)$ is found from (2.10) for the unmodified PB equation and from (3.16) for the modified PB equation. There is no slip at the wall, so the boundary conditions are

$$u(1) = 0 \tag{3.34}$$

and

$$\frac{\mathrm{d}u}{\mathrm{d}x} = 0 \quad \text{at} \quad x = 0. \tag{3.35}$$

The second boundary condition is again a result of the symmetry of the pore.

Viscosity

Two models are used for the viscosity μ. The first simply is a constant μ, as used by Berg and Findlay (2011) [3]. As was the case for the permittivity, this does not match the results from MD simulations. Using atomistic simulations to study a nano-scale channel filled with water and Cl^-, Freund [18] observed a shift in viscosity near the wall. There was an increase from a bulk value μ_b at the center of the pore to about 6 times the bulk value near the pore wall. In particular, the viscosity is large within roughly two molecular water layers at the wall. In this thesis, this shift is modeled based on the same equations as for the permittivity (3.13) [28] with a few minor changes. The profile for a $R = 20$Å pore is shown in figure 3.3. The equations used are

$$\mu(r) = A + B\tanh\left(\frac{|1-r| - sR}{kR}\right), \tag{3.36}$$

where s and k are fit parameters. A and B are constants given by

$$A = \mu_w + \frac{(\mu_b - \mu_w)\tanh(s/k)}{\tanh(s/k) + \tanh((1-s)/k)}, \tag{3.37}$$

$$B = \frac{(\mu_b - \mu_w)}{\tanh(s/k) + \tanh((1-s)/k)}. \tag{3.38}$$

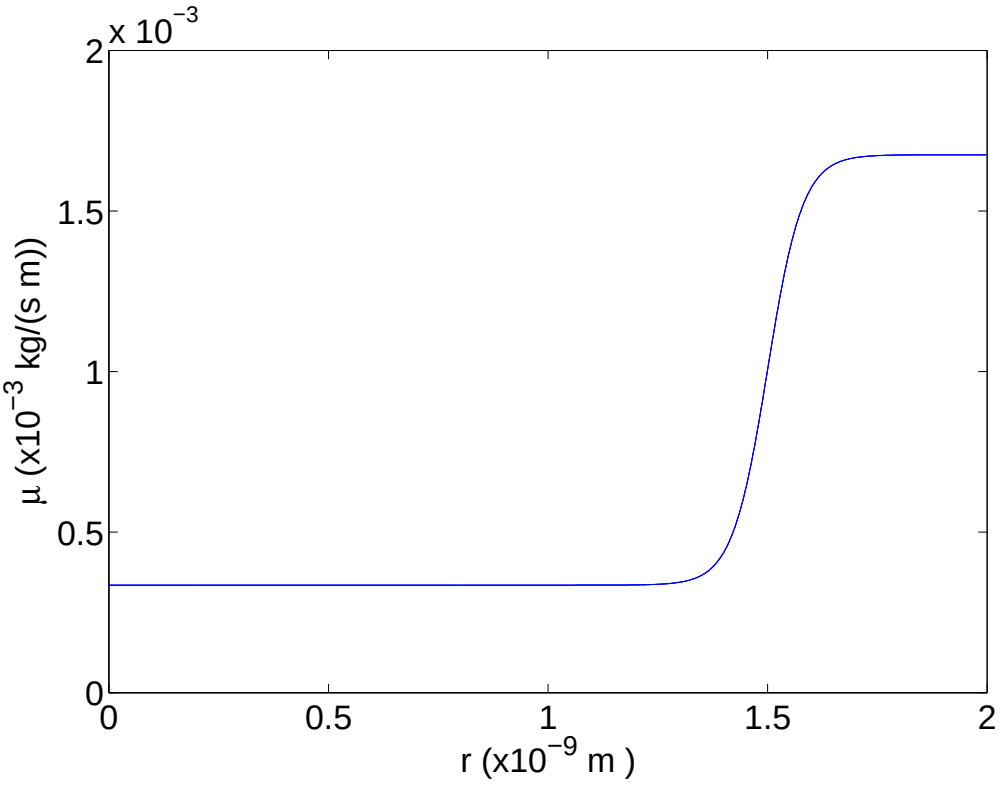

Figure 3.3: Profile of viscosity in a R=20Å pore. The value μ_w near the wall is 5 times larger than the bulk value μ_b. The fit parameters are $s = 0.5$ and $k = 0.08$.

3.5 Water Drag and Conductivity

To find the water drag η_{drag}, the total mass flux $\dot{M}$ through a cross section of the pore must be determined. Berg and Ladipo (2009) gives the mass flux as

$$\dot{M} = \int_0^r 2\pi[\rho u(r)]r\mathrm{d}r \tag{3.39}$$

where ρ is the water density. This can be expressed in non-dimensionalized variables as

$$\dot{M} = 2\pi\rho R^2 \int_0^1 xu(x)\mathrm{d}x \tag{3.40}$$

which can be evaluated numerically since $u(x)$ is known from the Stokes equation. For the integration we can use Simpson's rule, for example.

The proton flux J_+ is non-zero only in the z-direction. From (2.8) we can then write the total proton flux, or current as

$$J_+ = \int_0^R 2\pi \left[qc(r)u(r) + \frac{DF}{R_cT}qE_{\text{ext}}c(r)\right] rdr \tag{3.41}$$

which can be rewritten in non-dimensionalized variables as

$$J_+ = 2\pi R^2 \int_0^1 \left[qc(x)u(x) + \frac{DF}{R_c T} qE_{\text{ext}} c(x) \right] x dx. \tag{3.42}$$

The integral (3.42) can again be evaluated numerically.

The electro-osmotic drag η_{drag} is found from the ratio of the water flux and the proton flux as [4]

$$\eta_{drag} = \frac{\dot{M}}{\omega} \frac{F}{J_+}. \tag{3.43}$$

Here, the molar weight of water ω and Faradays constant F are included to convert both the water flux and proton flux to molar fluxes.

Finally, the pore conductivity σ_p can be written as [4]

$$\sigma_p = \frac{J_+}{\pi R^2 E_{\text{ext}}}. \tag{3.44}$$

4 Numerical Method

4.1 Solving the Poisson-Boltzmann Equation

As mentioned above, solving the PB equation is essentially a non-linear eigenvalue problem. The goal is to find the λ in (3.6) that matches the boundary condition (3.9) at the wall. In this work, a shooting method is used to match the boundary condition, starting with $\hat{\psi} = 0$ at $x = 0$ and marching forward to $x = 1$. Initially the value of λ is estimated and the potential $\hat{\psi}$ is solved, giving a value for (3.9). The derivative of the potential $\hat{\psi}'$ is monotonically increasing with λ. If the chosen λ yields a value for $\hat{\psi}'$ at the wall that is too high, the desired value for lambda must be lower than the chosen value. Conversely, if the value of $\hat{\psi}'$ is too low, λ must be higher. A higher and a lower bound for λ can be chosen initially and then updated as the derivative at the wall is found to be too large or too small (bisection method). The new guess for λ is then chosen to be $\lambda = (\lambda_h + \lambda_l)/2$ where λ_h and λ_l are the higher and lower bound, respectively. Repeating this, the value of λ that matches (3.9) can be found to a chosen precision, provided that the initial guess is large enough.

The procedure is identical for the first modified PB equation (3.17), but for the second modified PB equation (3.32), some care must be taken. Here, the permittivity is a function of the (actual) potential ψ and its derivative ψ', so the boundary condition (3.9) at the wall can no longer be used in the shooting method. To find a new wall condition for the shooting method which does not depend explicitly on ψ, the boundary condition (3.9) can be rearranged to yield

$$\frac{\mathrm{d}\hat{\psi}}{\mathrm{d}x}\varepsilon\left(\hat{\psi}(0), \hat{\psi}'(0)\right) = -\frac{Rq\sigma_s}{\varepsilon_0 c_0 k_b T} \qquad \text{at} \quad x = 1. \tag{4.1}$$

This new wall condition can then be used to match $\hat{\psi}'$, using the same procedure as described above.

The potential $\hat{\psi}$ is found using a fourth order Runge-Kutta scheme [40] for the shooting

method:

$$\begin{aligned} k_1 &= hf(x_n, y_n) \\ k_2 &= hf(x_n + \frac{1}{2}h, y_n + \frac{1}{2}k_1) \\ k_3 &= hf(x_n + \frac{1}{2}h, y_n + \frac{1}{2}k_2) \\ k_4 &= hf(x_n + h, y_n + k_3) \\ \Rightarrow y_{n+1} &= y_n + \frac{1}{6}k_1 + \frac{1}{3}k_2 + \frac{1}{3}k_3 + \frac{1}{6}k_4, \end{aligned} \tag{4.2}$$

where we set

$$v = \hat{\psi} \tag{4.3}$$

and

$$w = v' \tag{4.4}$$

and solve the resulting first-order ODE system

$$v' = w \tag{4.5}$$

and

$$w' = \hat{\psi}''. \tag{4.6}$$

Here, $\hat{\psi}''$ is the right hand side of the corresponding PB equation above.

The computed potential $\hat{\psi}$ is then used to find the proton distribution $c(x)$ in the pore from (2.10) for the unmodified PB equation or (3.16) for the modified PB equations. This is in turn used to solve the Stokes equation (3.33).

4.2 Stokes Equation, Water Drag and Conductivity

The Stokes equation (3.33) can be solved linearly. The differentiation in (3.33) yields

$$\mu\frac{\mathrm{d}u}{\mathrm{d}x} + \frac{\mathrm{d}\mu}{\mathrm{d}x}x\frac{\mathrm{d}u}{\mathrm{d}x} + \mu x\frac{\mathrm{d}^2u}{\mathrm{d}x^2} = PR^2x - qc(x)ER^2x \tag{4.7}$$

or

$$\frac{\mathrm{d}^2u}{\mathrm{d}x^2} + \frac{\mathrm{d}u}{\mathrm{d}x}\left(\frac{\mathrm{d}\mu}{\mathrm{d}x}\frac{1}{\mu} + \frac{1}{x}\right) = \frac{PR^2 - qc(x)ER^2}{\mu}. \tag{4.8}$$

Now, (4.8) with boundary conditions (3.34) and (3.35) can be discretized according to

$$\frac{\mathrm{d}^2u}{\mathrm{d}x^2} \approx \frac{u_{i+1} - 2u_i + u_{i-1}}{h^2} \quad \text{at} \quad x = x_i, \tag{4.9}$$

$$\frac{\mathrm{d}u}{\mathrm{d}x} \approx \frac{u_{i+1} - u_{i-1}}{2h} \quad \text{at} \quad x = x_i, \tag{4.10}$$

$$\frac{\mathrm{d}u}{\mathrm{d}x} \approx \frac{-3u_0 + 4u_1 - u_2}{2h} \quad \text{at} \quad x = x_0, \tag{4.11}$$

yielding $\left(\frac{\mathrm{d}\mu}{\mathrm{d}x_i} = \frac{\mathrm{d}\mu}{\mathrm{d}x} \quad \text{at} \quad x = x_i\right)$

$$\frac{u_{i+1} - 2u_i + u_{i-1}}{h^2} + \left(\frac{\mathrm{d}\mu}{\mathrm{d}x_i}\frac{1}{\mu(x_i)} + \frac{1}{x_i}\right)\frac{u_{i+1} - u_{i-1}}{2h} = \frac{PR^2 - qc(x_i)ER^2}{\mu(x_i)} \qquad (i \neq 0, N), \tag{4.12}$$

$$\frac{-3u_0 + 4u_1 - u_2}{2h} = 0 \qquad (i = 0), \tag{4.13}$$

$$u_i = 0 \qquad (i = N). \tag{4.14}$$

Rearranging (4.12) gives

$$\left(\frac{1}{h^2} - \frac{\frac{\mathrm{d}\mu}{\mathrm{d}x_i}\frac{1}{\mu(x_i)} + \frac{1}{x_i}}{2h}\right)u_{i-1} - \left(\frac{2}{h^2}\right)u_i + \left(\frac{1}{h^2} + \frac{\frac{\mathrm{d}\mu}{\mathrm{d}x_i}\frac{1}{\mu(x_i)} + \frac{1}{x_i}}{2h}\right)u_{i+1} = \frac{PR^2 - qc(x_i)ER^2}{\mu(x_i)}. \tag{4.15}$$

This can be written as a system of linear equations

$$\begin{aligned} A_i u_{i-1} + B_i u_i + C_i u_{i+1} &= F_i, \quad i = 1, ..., N-1 \\ A_0 u_0 + B_0 u_1 + C_0 u_2 &= 0 \\ A_N u_{N-2} + B_N u_{N-1} + C_N u_N &= 0 \end{aligned} \tag{4.16}$$

or

$$M\boldsymbol{u} = \boldsymbol{F} \tag{4.17}$$

where $\boldsymbol{u} = (u_0, u_1, ..., u_N)^T$ and $\boldsymbol{F} = 0, F_1, ..., F_{N-1}, 0$. The matrix M is given as

$$M = \begin{bmatrix} A_0 & B_0 & C_0 & 0 & 0 & .... & 0 \\ A_1 & B_1 & C_1 & 0 & 0 & .... & 0 \\ 0 & A_2 & B_2 & C_2 & 0 & .... & 0 \\ ... & ... & ... & ... & ... & ... & ... \\ 0 & 0 & 0 & 0 & A_{N-1} & B_{N-1} & C_{N-1} \\ 0 & 0 & 0 & 0 & A_N & B_N & C_N \end{bmatrix} \tag{4.18}$$

where

$$A_0 = \frac{-3}{2h}$$
$$B_0 = \frac{4}{2h}$$
$$C_0 = \frac{-1}{2h}$$

$$
\begin{aligned}
A_i &= \frac{1}{h^2} - \frac{\frac{\mathrm{d}\mu}{\mathrm{d}x_i}\frac{1}{\mu(x_i)} + \frac{1}{x_i}}{2h} \\
B_i &= \frac{-2}{h^2} \\
C_i &= \frac{1}{h^2} + \frac{\frac{\mathrm{d}\mu}{\mathrm{d}x_i}\frac{1}{\mu(x_i)} + \frac{1}{x_i}}{2h}
\end{aligned}
\tag{4.19}
$$

$$
\begin{aligned}
A_N &= 0 \\
B_N &= 0 \\
C_N &= 1
\end{aligned}
$$

The fluid velocity $u(r)$ can now be found in a straightforward manner by solving (4.17).

Finally, the integrals for the proton flux J_+ in (3.41) and the mass flux in (3.40) can be evaluated numerically using a Simpson's rule solver according to [40]

$$
\int_{x_0}^{x_N} f(x)dx = h\left[\frac{1}{3}f_0 + \frac{4}{3}f_1 + \frac{2}{3}f_2 + \frac{4}{3}f_3 + \cdots + \frac{2}{3}f_{N-2} + \frac{4}{3}f_{N-1} + \frac{1}{3}f_N\right] \tag{4.20}
$$

The water drag and pore conductivity can then be determined from (3.43) and (3.44), respectively.

5 Results and Discussion

Parameter	Description	Value
a	Effective size of H_3O^+	2.2 Å to 3.14 Å
D	Diffusion coefficient of protons	7.5 x 10^{-10} m^2 s^{-1}
E_{ext}	Applied electric field	2000 V m^{-1}
T	Temperature	353 K
ε_b	Bulk permittivity of water	60.93
ε_w	Permittivity of water at the wall	8
μ_b	Bulk viscosity of water	3.35 x 10^{-4} Pa s
ρ	Water density	971.8 kg m^{-3}

Table 5.1: Values of system parameters

5.1 Proton Concentration

Figure 5.1 shows what effect the introduction of finite-size ions in the PB-equation has on the concentration $c(x)$ of protons in the pore when the permittivity is kept constant at bulk value. As the concentration approaches the maximum concentration allowed, $a^{-3} = 9.36$ x 10^{28} m^{-3}, the distribution should flatten out. For the surface charge density $\sigma_s = -0.1$, the distributions in figure 5.1 are too low for the modification (3.16) to matter and the two curves coincide. For $\sigma_s = -0.5$ C m^{-2} the modified concentration near the wall is suppressed, leaving a slightly larger concentration in the rest of the pore.

In figure 5.2 a varying permittivity $\varepsilon(r)$ (see figure 3.2) is introduced, resulting in a significantly higher concentration near the wall where ε is small. For $\sigma_s = -0.5$ C m^{-2}, this has the effect of a more pronounced flattening of the distribution at the wall compared to the constant permittivity distribution in figure 5.1. The profile of the distributions changes markedly with the introduction of a varying permittivity. The

concentration of protons is higher in areas of low permittivity, that is near the walls, while the concentration near the center of the pore is lower.

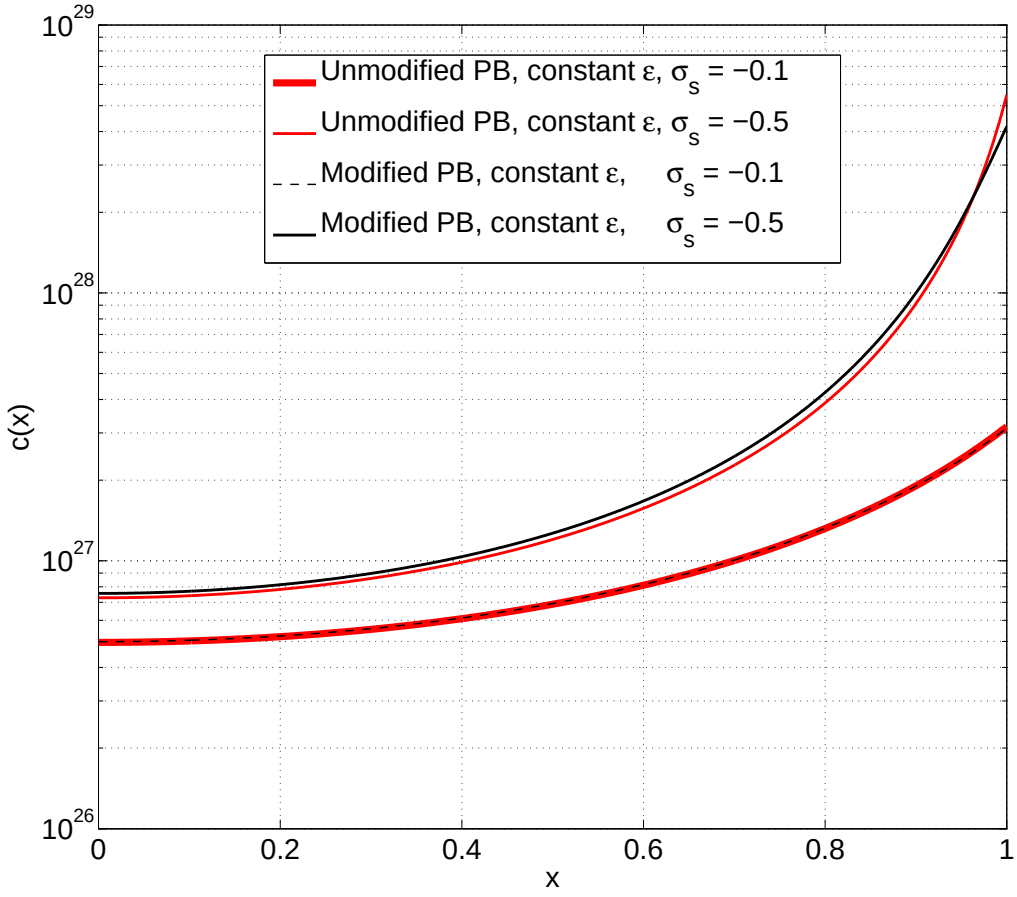

Figure 5.1: Concentration of protons as a function of position x in a 1 nm pore for both the modified PB equation and the unmodified PB equation with constant permittivity and $\sigma_s = -0.5$ and $\sigma_s = -0.1$ (in C m^{-2}).

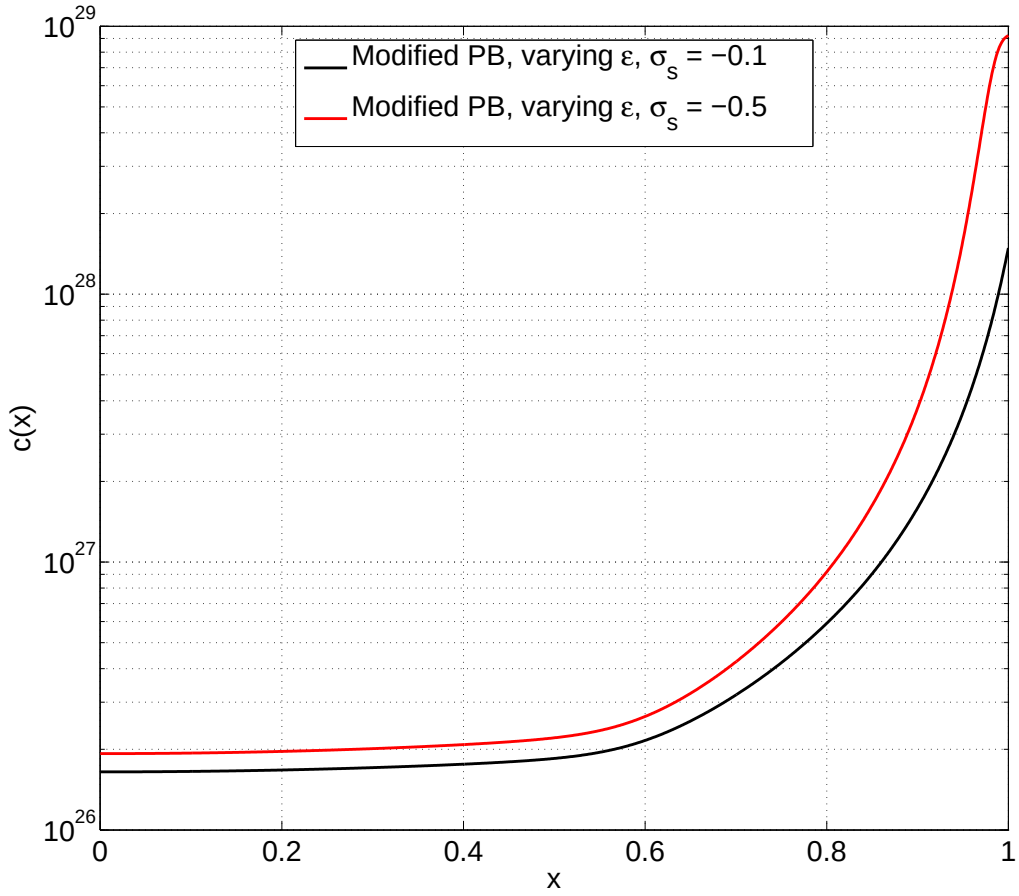

Figure 5.2: Concentration of protons as a function of position x in a 1 nm pore for the modified PB equation with varying permittivity and $\sigma_s = -0.5$ and $\sigma_s = -0.1$ (in C m^{-2}).

5.2 Water Drag

The water drag is a characteristic quantity of the PEM that is measurable experimentally. It is therefore of interest to compare the values presented here with experimental results. Also of interest is the effect each modification made to the model, that is the inclusion of finite-size ions, the non-constant permittivity and the non-constant viscosity, has on the results. Figures 5.3 to 5.6 show the dependency of the water drag coefficient η_{drag} on the radius R of the pore for different values of the pressure gradient P and the surface charge density σ_s. Results are found using different modifications to the PB equation and Stokes equation. The values chosen for σ_s, -0.1 and -0.5 C m^{-2}, should represent the limits for the surface charge density of a typical PEM.

The water drag is in general found to be increasing with increasing pore radius R. For very large pressure gradients, around $P = 10^{11}$Pa m^{-1} [16], the effect of the pressure gradient on the flow increases, and the drag coefficient can turn negative, meaning the flow of water opposes the flow of protons. This effect seems to become more important the smaller the surface charge density σ_s of the pore is. A negative drag coefficient corresponds to back diffusion in the pore [3]. These findings are a result of a parabolic-like water velocity profile, where the maximum velocity is found at the pore center, while most protons are found near the walls where u is very small.

The results in figures 5.3 and 5.4 are found using the unmodified PB equation in (3.6) and the modified PB equation in (3.17) respectively, with constant permittivity and viscosity at bulk value. The only difference between the two is then the inclusion of finite size-ions in figure 5.4. For $\sigma_s = -0.1$ C m^{-2} there is no discernible difference when including finite-size ions. This is as expected, considering the distribution of protons shown in figure 5.1, was largely unaffected by the modification. Increasing the surface charge density to $\sigma_s = -0.5$ C m^{-2}, the difference is still marginal. The water drag turns negative for $\sigma_s = -0.1$ C m^{-2} and $P = 10^{11}$ Pa m^{-1}, but only when the channel radius is relatively large.

In figure 5.5, a varying permittivity with the profile from figure 3.2 is included in the modified PB model. The effect of this inclusion is to lower values for the water drag coefficient η_{drag} all over. This is especially true for large pressure gradients where the turn to negative values of η_{drag} happens for smaller R. As a result, the value of η_{drag} at $R = 1$ nm for $\sigma_s = -0.1$ C m^{-2} and $P = 10^{10}$ Pa m^{-1} is about a third of the value for the constant permittivity case. For smaller pressure gradients, there is a 20-30% drop in η_{drag} at $R = 1$ nm. Another notable effect is the turn to negative values of η_{drag} for large σ_s at $P = 10^{10}$ Pa m^{-1}.

In figure 5.6, a varying viscosity with the profile from figure 3.3 is included in the modified PB model in addition to the non-constant permittivty. This inclusion has the effect of further lowering the values for η_{drag}. At $R = 1$ nm and $P = 0$ and $P = 10^{10}$ Pa m^{-1}, the values for η_{drag} are reduced by about a factor of 4 compared to the case with constant permittivity and viscosity. For $P = 10^{11}$ Pa m^{-1}, η_{drag} is seen to turn

negative at smaller R. This results in a value of η_{drag} for $\sigma_s = -0.1$ C m^{-2} that is an order of magnitude lower compared to the constant permittivity and viscosity case. For $\sigma_s = -0.5$ C m^{-2}, the value is reduced by a factor of 5.

To isolate the effect of the protons on the flow of water, η_{drag} should be measured when $P = 0$. Experimental and theoretical studies indicate a value of η_{drag} between 1 and 3 [34, 51]. For the case of constant permittivity in figures 5.3 and 5.4, the values for η_{drag} at $R = 1$ nm are about 7.5 and 22 for $\sigma_s = -0.5$ and -0.1 C m^{-2}, respectively. The values are almost identical for the unmodified and modified PB equation. These values line up with Berg and Findlay [3], who found a value around 15 from an analytical solution of the PB and Stokes equation with constant permittivity and viscosity. Introducing a varying permittivity, the values of η_{drag} for the same pore decrease to about 6 and 17 for $\sigma_s = -0.5$ and -0.1 C m^{-2}, respectively. Finally, adding a varying viscosity yields values of about 2 and 5 for $\sigma_s = -0.5$ and -0.1 C m^{-2} respectively. This is close to the experimental values. It is also apparent that the inclusion of a varying permittivity and viscosity greatly improve the results, as predicted by Berg and Findlay [3]. The effect of the finite-size ions looks to be limited, although the concentration is significantly higher near the wall with the varying permittivity as seen in figure 5.2, so it might make a difference for large σ_s.

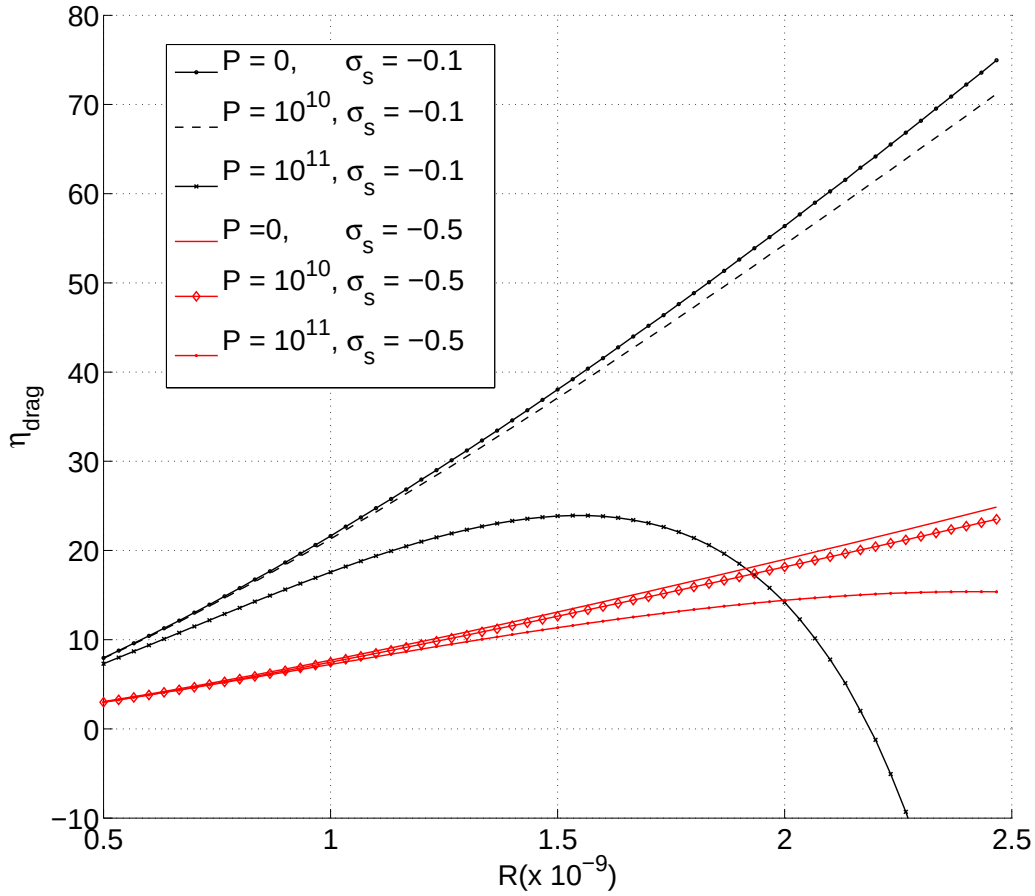

Figure 5.3: Water drag η_{drag} as a function of pore radius R for the unmodified PB equation (3.1) with constant (bulk) values for permittivity and viscosity. Values are found for surface charge densities $\sigma_s = -0.1$ and $\sigma_s = -0.5$ (in C m^{-2}) and different values for the constant pressure gradient P (in Pa m^{-1}).

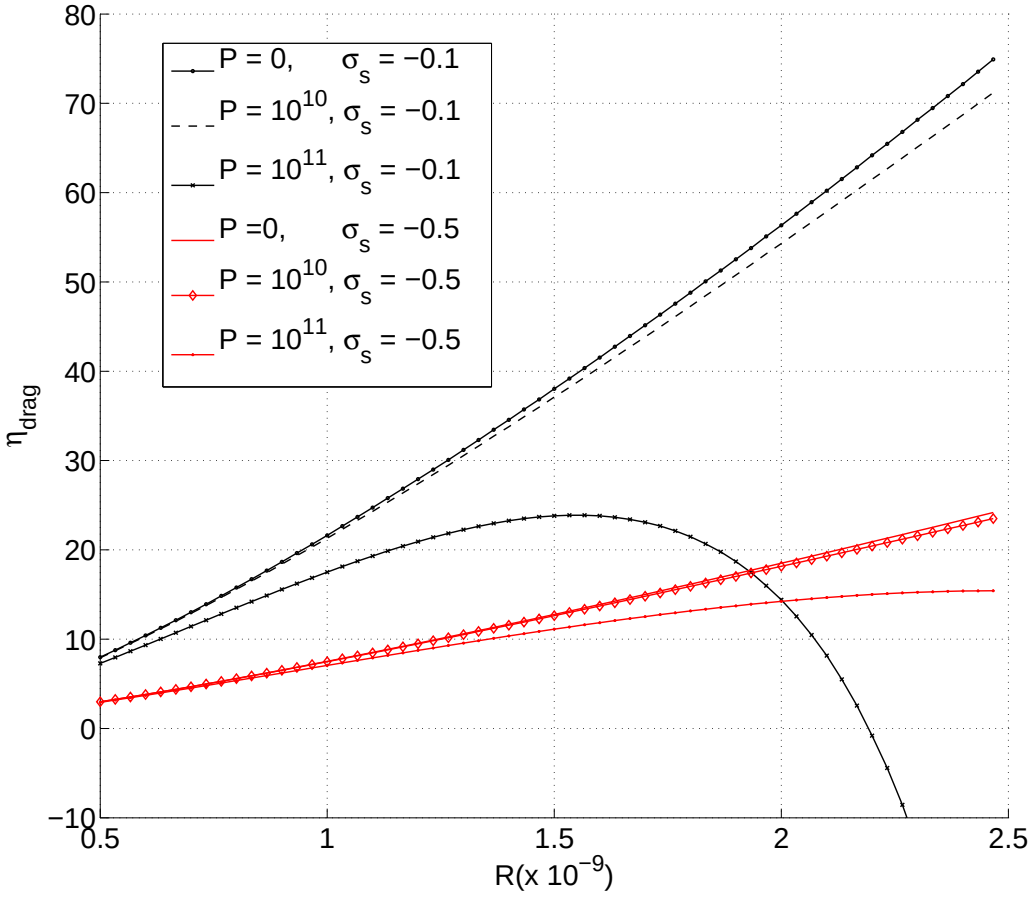

Figure 5.4: Water drag η_{drag} as a function of pore radius R for the modified PB equation (3.17) with constant (bulk) values for permittivity and viscosity. Values are found for surface charge densities $\sigma_s = -0.1$ and $\sigma_s = -0.5$ (in C m^{-2}) and different values for the constant pressure gradient P (in Pa m^{-1}).

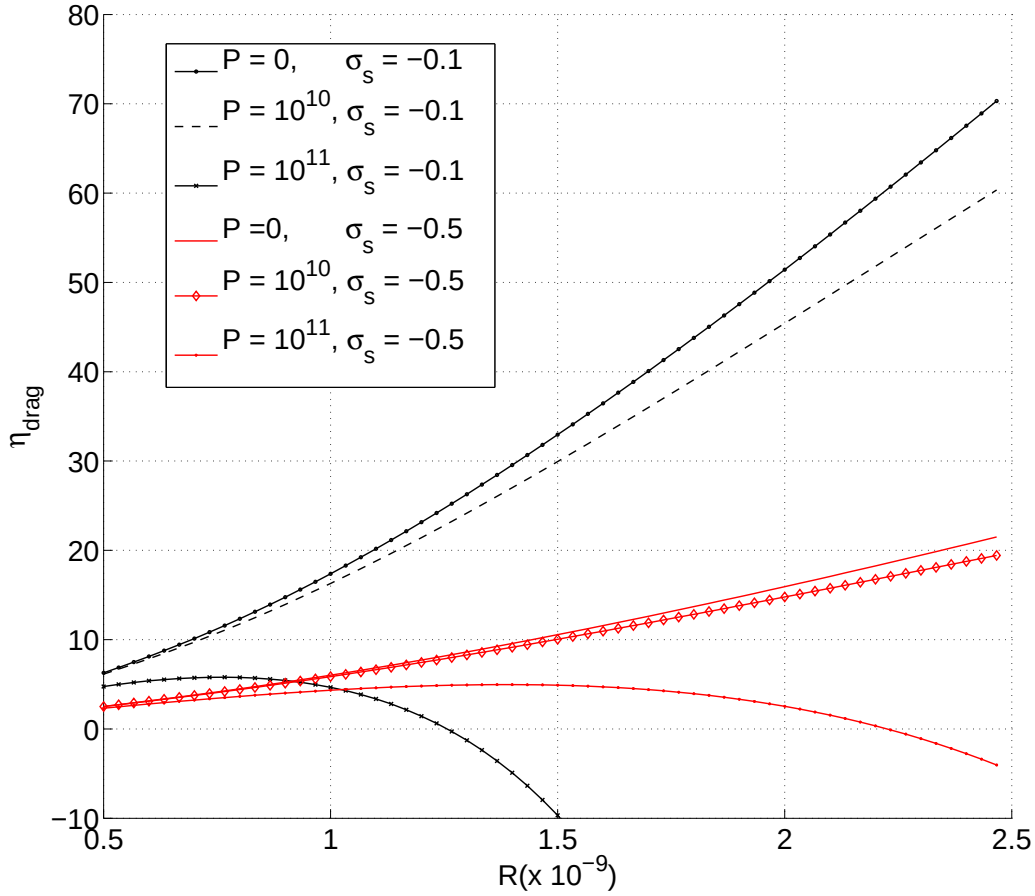

Figure 5.5: Water drag η_{drag} as a function of pore radius R for the modified PB equation (3.17) including varying permittivity with the profile from figure 3.2 and constant (bulk) viscosity. Values are found for surface charge densities $\sigma_s = -0.1$ and $\sigma_s = -0.5$ (in C m^{-2}) and different values for the constant pressure gradient P (in Pa m^{-1}).

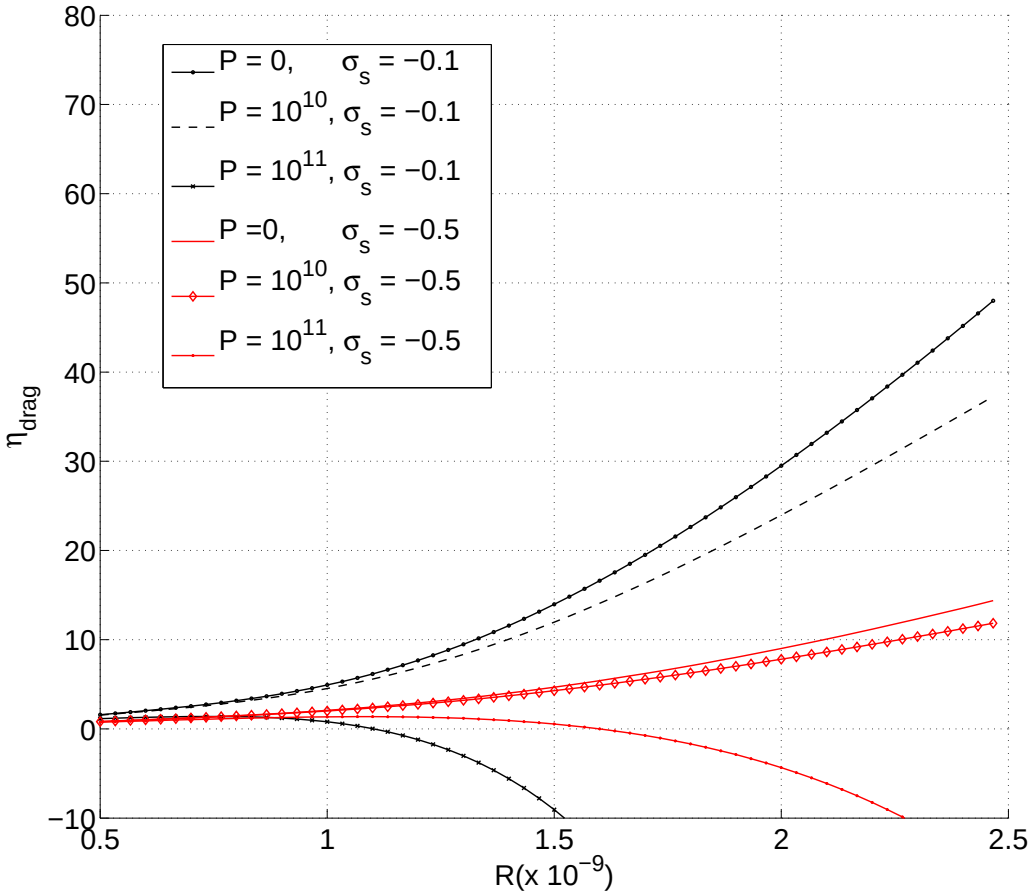

Figure 5.6: Water drag η_{drag} as a function of pore radius R for the modified PB equation (3.17) including varying permittivity with the profile from figure 3.2 and varying viscosity with the profile from figure 3.3. Values are found for surface charge densities $\sigma_s = -0.1$ and $\sigma_s = -0.5$ (in C m^{-2}) and different values for the constant pressure gradient P (in Pa m^{-1}).

5.3 Pore Conductivity

The second quantity studied is the pore conductivity σ_p, which can also be measured experimentally. As was the case for the water drag, the objective is to compare the results with experimental data and observe the difference each modification to the PB model makes to the conductivity. Figures 5.7 to 5.10 show the dependency of the pore conductivity σ_p on the radius R of the pore for different values of the pressure gradient P and the surface charge density σ_s. Results are found using different modifications to the PB equation and Stokes equation.

In general, the pore conductivity falls as the pore radius R increases since c decreases. The pressure gradient P only matters when very large ($P = 10^{11}$), and even then the effect is limited, especially with non-constant permittivity and viscosity as seen in figure 5.10. A larger surface charge density σ_s results in larger values for σ_p. This is perhaps not surprising, considering this also means a larger overall proton concentration in the pore.

In figure 5.7 the results are found using the unmodified PB equation (3.6), whereas the results in figure 5.8 are found using the modified PB equation (3.17) with finite-size ions. Both the permittivity and the viscosity are kept constant at bulk value. As was the case with the water drag, there is no discernible effect for small surface charge densities. For $\sigma_s = -0.5$, the values for σ_p at $R = 1$ nm are a bit larger for the modified PB equation than for the unmodified PB equation.

The results when including the variable permittivity from figure 3.2, can be seen in figure 5.9. The value of σ_p at 1 nm is reduced by a factor of 2 for $\sigma_s = -0.5$ C m^{-2} and close to 2 for $\sigma_s = -0.1$ C m^{-2}. In figure 5.10, the variable viscosity from figure 3.3 is added to the model. At $R = 1$ nm, this further reduces σ_p by about 40% for $\sigma_s = -0.5$ C m^{-2}, while the reduction is somewhat less for $\sigma_s = -0.1$ C m^{-2}.

Experimental data puts σ_p at around 6 S m^{-1} [35] for Nafion. Measuring at $P = 0$ and $R = 1$ nm, the values of σ_p for the constant permittivity cases are around 13 and 100 S m^{-2} for $\sigma_s = -0.1$ and -0.5 C m^{-2}, respectively. Including the varying permittivity puts the same values at around 7 and 50 S m^{-1}. Finally, including also the variable viscosity reduces the values to about 5.5 and 30 S m^{-1}. For small σ_s, the results when including the non-constant permittivity and viscosity, are very reasonable compared to the experimental data. For the larger surface charge density $\sigma_s = -0.5$ C m^{-2}, the values are significantly larger than the experimental reference, but not completely unreasonable. It is clear that the introduction of varying permittivity and viscosity significantly improved the results for the pore conductivity. The values are lower by a factor 2 or more compared to the unmodified case. The effect of the finite-size ions seems to be larger than for the water drag, although at constant permittivity it has the effect of increasing the conductivity. This might not be the case for the varying permittivity. The integral for the proton flux (3.42) in the pore conductivity (3.44) includes both the concentration $c(x)$ of protons and the fluid velocity $u(x)$. From

inspection of the figure 5.1, it is apparent that the concentration for the modified PB equation is lower than the unmodified PB concentration only at the wall where the velocity u is close to zero (from the no-slip boundary condition). This might explain the slightly larger value.

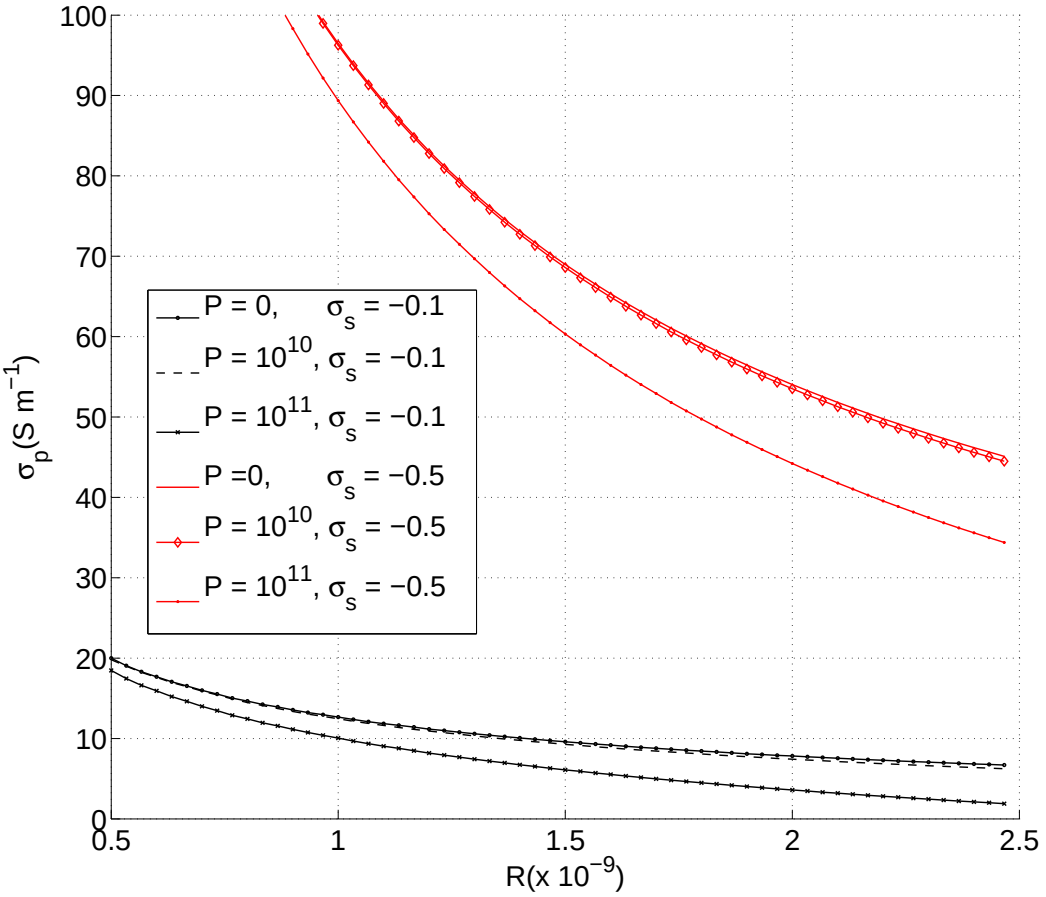

Figure 5.7: Pore conductivity σ_p as a function of pore radius R for the unmodified PB equation (3.1) with constant (bulk) values for permittivity and viscosity. Values are found for surface charge densities $\sigma_s = -0.1$ and $\sigma_s = -0.5$ (in C m^{-2}) and different values for the constant pressure gradient P (in Pa m^{-1}).

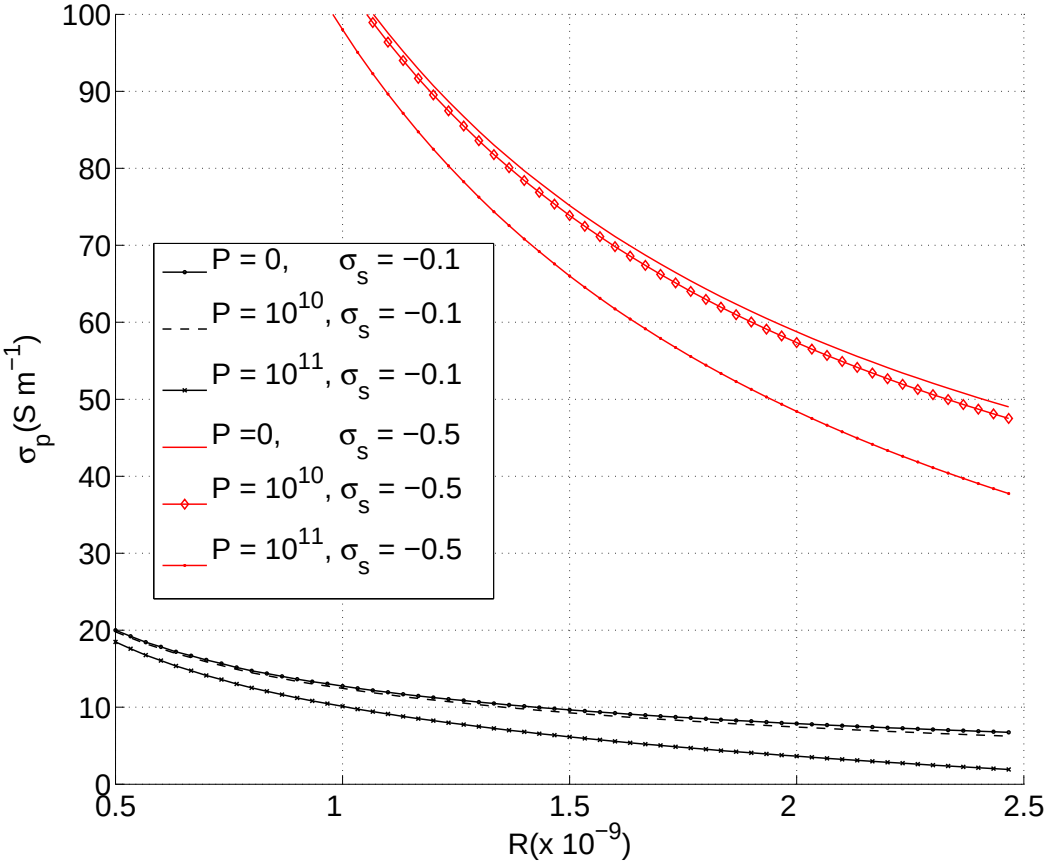

Figure 5.8: Pore conductivity σ_p as a function of pore radius R for the modified PB equation (3.17) with constant (bulk) values for permittivity and viscosity. Values are found for surface charge densities $\sigma_s = -0.1$ and $\sigma_s = -0.5$ (in C m^{-2}) and different values for the constant pressure gradient P (in Pa m^{-1}).

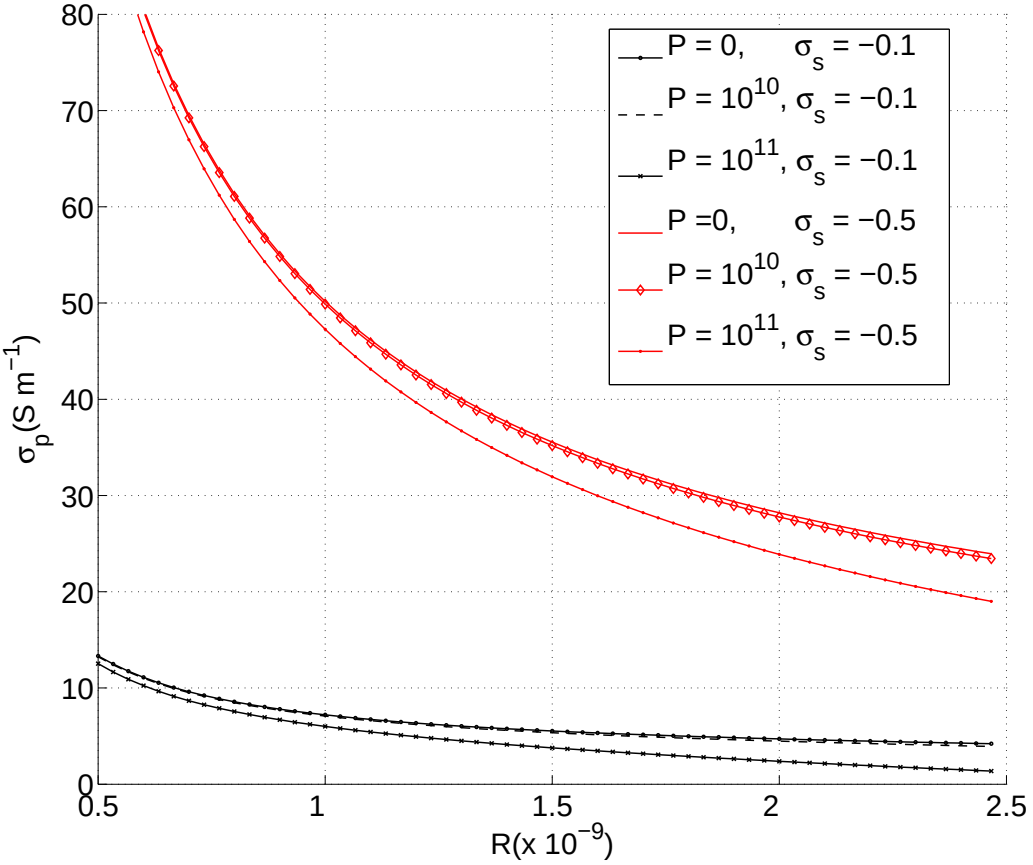

Figure 5.9: Pore conductivity σ_p as a function of pore radius R for the modified PB equation (3.17) including varying permittivity with the profile from figure 3.2 and constant (bulk) viscosity. Values are found for surface charge densities $\sigma_s = -0.1$ and $\sigma_s = -0.5$ (in C m^{-2}) and different values for the constant pressure gradient P (in Pa m^{-1}).

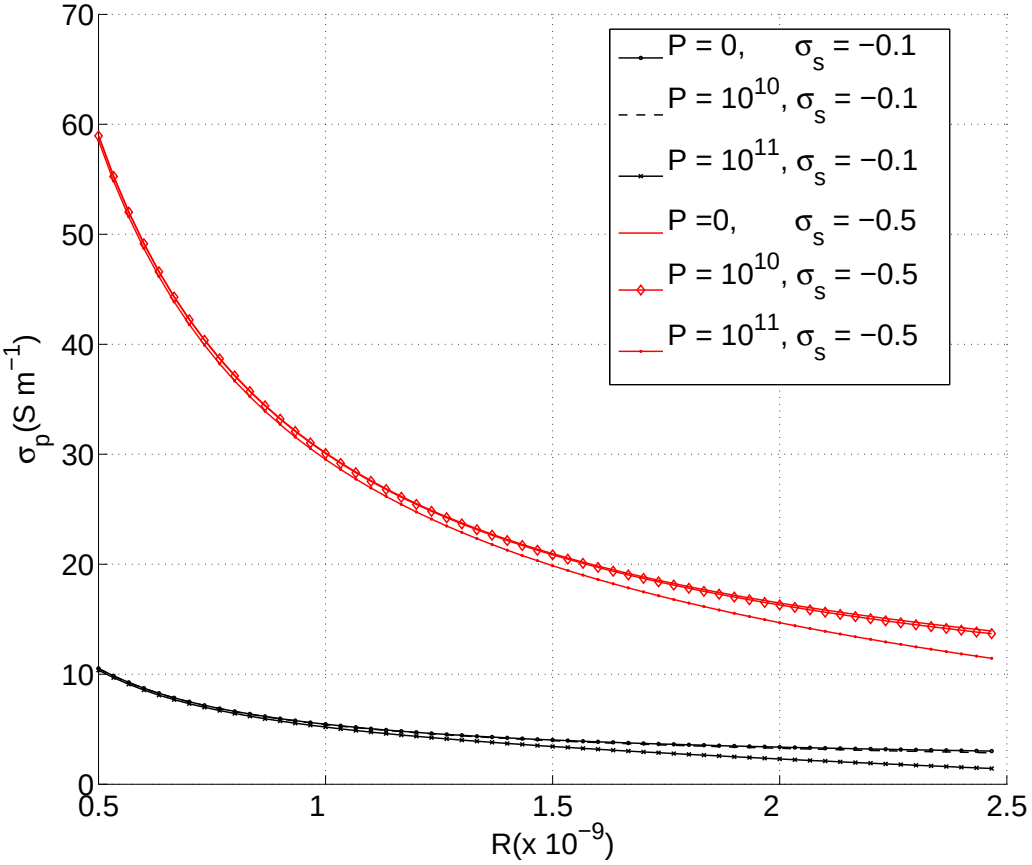

Figure 5.10: Pore conductivity σ_p as a function of pore radius R for the modified PB equation (3.17) including both a varying permittivity with the profile from figure 3.2 and a varying viscosity with the profile from figure 3.3. Values are found for surface charge densities $\sigma_s = -0.1$ and $\sigma_s = -0.5$ (in C m^{-2}) and different values for the constant pressure gradient P (in Pa m^{-1}).

5.4 Modified Poisson-Boltzmann Equation with Explicit Model for Permittivity

The modified Poisson-Boltzmann equation (3.23) with the explicit model for permittivity from (3.22) introduces a permittivity depending explicitly on the potential ψ and the local electric field $E = -\psi'$. Since the model is based on the ordering of water dipoles, finding the correct spatial variation of the number density, or concentration, of water in (3.21) is essential to achieve accurate results. This variation stems directly form the variation in the concentration of protons, as all protons are assumed to appear as H_3O^+ ions. Coupling this to the finite-size ion modification from (3.17), the effective size a chosen for the H_3O^+ ions becomes important. In the first modified PB equation (3.17), this size was chosen to be a bit smaller than the effective size of the water molecules. Attempting to use the same size for the current model, one could end up with a larger number density of protons near the wall than the number density n_0 of water with no protons present. This would appear as a negative n_w in (3.21), which would not be physical and cause a breakdown of the shooting method used to match the wall condition (3.9). To gain an understanding of the qualitative properties of the model, a new effective size a was chosen so that the H_3O^+ ion would be slightly larger than a water molecule, thereby eliminating the possibility of negative n_w. However, large concentrations of protons, as seen near the walls, would still lead to a depletion of water molecules. With the model (3.22), where the magnitude of the effective dipole moment of hydronium is taken to be zero, this will result in a very small permittivity.

Figure 5.11 shows the effective permittivity ε_{eff} as a function of the position x in a 1 nm pore for different values of the surface charge density σ_s. The permittivity is found to be almost constant up to a point at around $x = 0.75$ where it starts to decrease rapidly ending up at around 1, which is the lowest value allowed in (3.19). The shift from bulk value to 1 occurs at larger x as σ_s is decreased. For $\sigma_s = -0.1$, the shift does not happen at all, and the value of the permittivity is about 58 at the wall. The profile for large σ_s is qualitatively not very different from the profile used in the first modified PB equation (see figure 3.2). The wall and bulk values are different, however. In addition, the shift from bulk value to the wall value of the permittivity happens closer to the wall in the explicit model. The position of the shift in figure 3.2 is based on the work of Paul and Paddison [37, 36].

Figure 5.12 shows the effective permittivity as a function of the pore potential $\hat{\psi}$ for a given $\hat{\psi}'$. This profile shares the characteristic shift from bulk to wall values of the permittivity with the positionally dependent plots in figure 5.11. The value of the permittivity at the wall is expected to be around 10 [36]. Achieving such a value with this model would be difficult. The shift happens over a short interval in the potential, but near the wall, the derivative of the potential $\frac{\mathrm{d}\hat{\psi}}{\mathrm{d}x}$ is large. In practice, this means that the permittivity at the wall will most likely either be large (> 40) or hit the lower limit for the permittivity (~ 1). Therefore a more realistic permittivity model is called

for that captures the dynamics of protonated water complexes near the wall.

The plots in figure 5.13 show the concentration of protons $c(x)$ as a function of position x in a $R = 1$ nm pore for decreasing values of the surface charge density σ_s. For large surface charge densities, the concentration reaches the maximum allowed concentration (a^{-3}) at a distance of about 1 Å from the wall. As σ_s decreases, the concentration reaches the maximum value closer to the wall. For $\sigma_s = -0.1$ C m^{-2}, the concentration never reaches the maximum. In comparison with figure 5.11, the concentration seems to reach the maximum value at the same distance from the wall as the permittivity reaches its minimum. Figure 5.2 showed that a lower permittivity near the wall allows for a higher concentration of protons, so this is perhaps not surprising. Since the effective size a of the protons is larger in the explicit model, the maximum concentration is lower than for the first modified PB equation. This saturation in the concentration also resembles the distribution one might expect with a Stern layer present [13].

As the model is implemented at the moment, the number concentration of water $n_w(x)$ at the center of the pore is taken to be $n_w(0) = n_0$ so as to enable the calculation of the permittivity at the pore center, $\varepsilon(0)$. This is not strictly true, as the concentration of protons at the center, $c(0)$, is nonzero. The error this introduces in $n_w(0)$ is roughly 3%. This is reduced somewhat, as a lower n_{w0} gives a lower $\varepsilon(0)$, and in turn a lower $c(0)$. Another loose end is the effective magnitude of the water dipole moment p_0 which was taken to be $p_0 = 4.79$ D by Gongadze *et al.* [22]. Using this value for p_0, the bulk permittivity is from (3.19) found to be around 65, about 10% higher than the actual bulk value at $T = 353$K. A recalibration of p_0 at $T = 353$K could mitigate this.

Because of the issues with the model, no plots for the water drag η_{drag} and pore conductivity σ_p have been included here. However, for comparison with the other models, values have been found for 1 nm pores with the variable viscosity included. The water drag was found to be between about 3 and 9 for surface charge densities $\sigma_s = -0.1$ to -0.5 C m^{-2}. This is slightly larger than the values for the first modified PB equation with variable permittivity. The values for the pore conductivity are found to be between about 7 and 100 for $\sigma_s = -0.1$ to -0.5 C m^{-2}. This is larger than in the previous model. The conductivity also seems to be more sensitive to changes in the surface charge density.

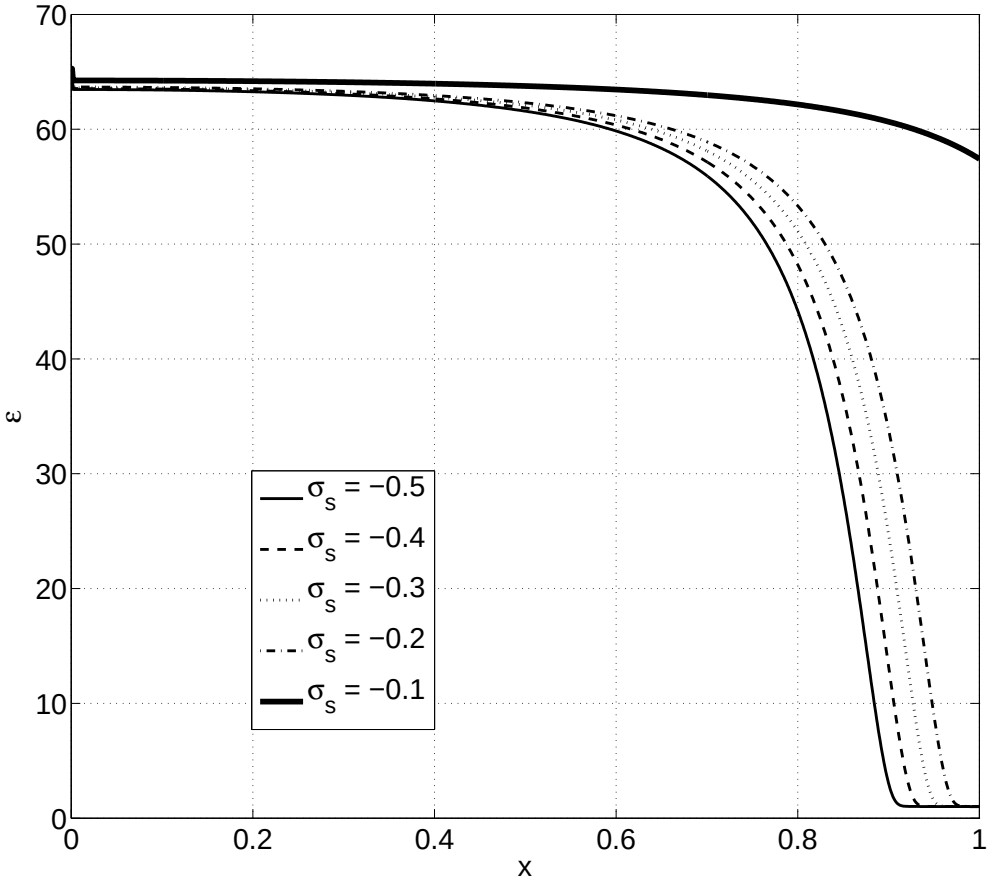

Figure 5.11: Value of the permittivity ε_{eff} as a function of position x in a $R = 1$ nm pore for decreasing values of the surface charge density σ_s .

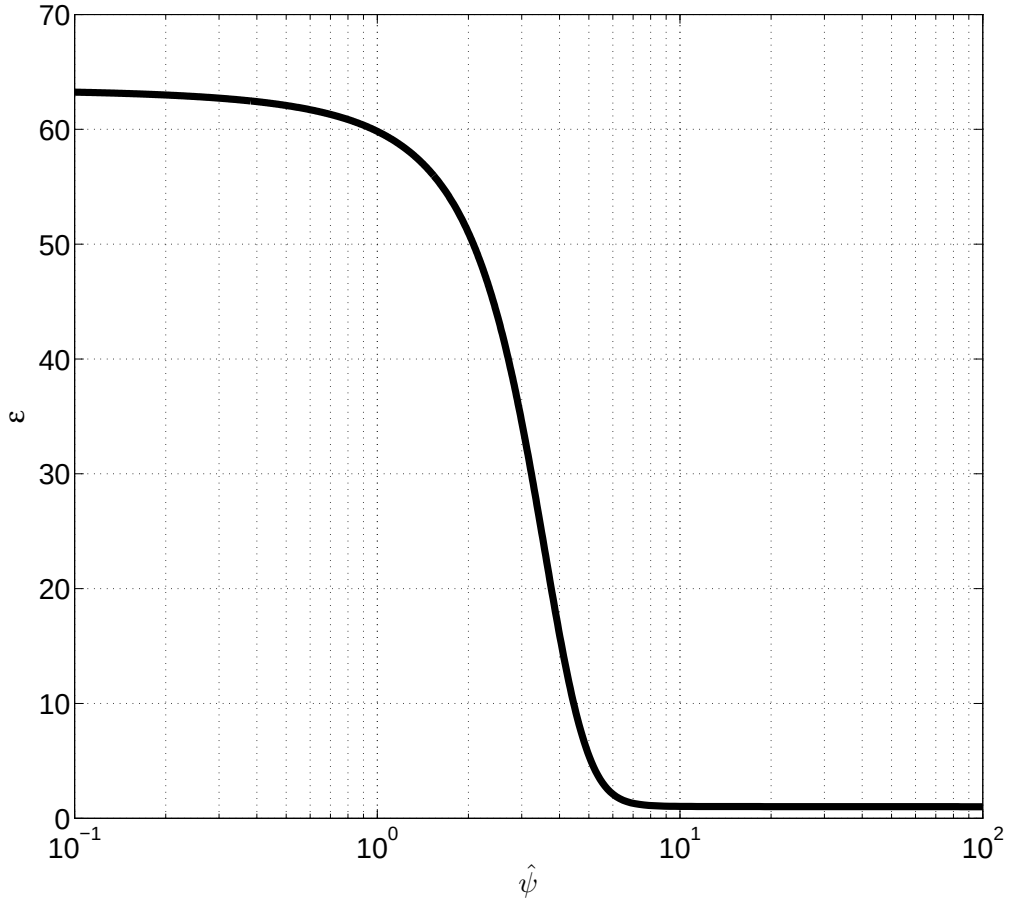

Figure 5.12: Value of the permittivity ε_{eff} as a function of the potential $\hat{\psi}$ for a given $\hat{\psi}'$.

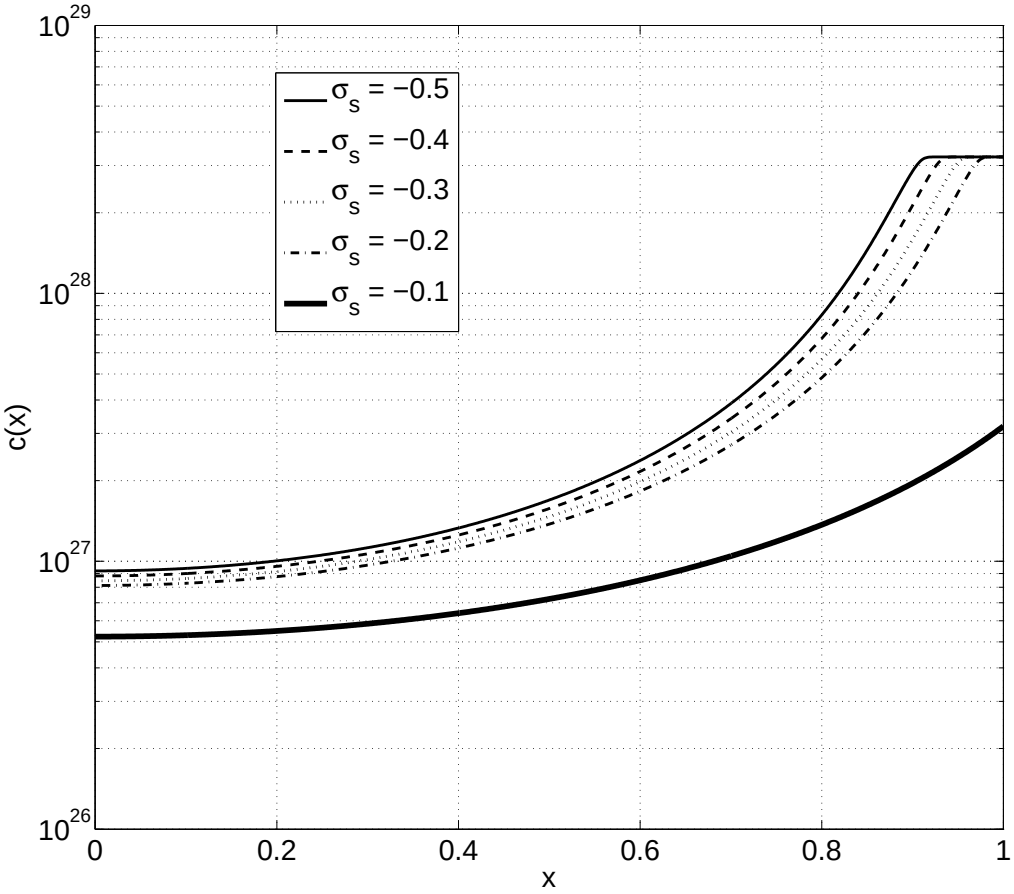

Figure 5.13: Concentration of protons $c(x)$ as a function of position x in a $R = 1$ nm pore for decreasing values of the surface charge density σ_s.

6 Conclusion and Outlook

6.1 Conclusion

The main goal of this thesis was to study the effects of different modifications made to the PB and Stokes equations for electro-osmotic flow in nano-scale pores reminiscent of the pores found in PEM membranes. As such, the inclusion of finite-size ions in the PB equation (3.17) had modest effects when applied to a system with constant permittivity. Adding a positionally dependent permittivity where the value, based on microscopic simulations found in literature, dropped near the pore surface, increased the wall concentration of protons and thereby the effect of the finite-size ion modification. Values for both the water drag coefficient and the pore conductivity were reduced significantly, coming closer to experimental values. Including a similar model for the viscosity, with an increased value only near the wall instead of a gradually increasing profile, yielded even better results for the water drag and pore conductivity when compared to experimental values. The water drag coefficient attained values between 2 and 5 for surface charge densities $\sigma_s = -0.1$ to -0.5 C m^{-2} which is very close to the experimental reference values of 1-3. Values were about a factor four lower than the unmodified PB results. The pore conductivity gave values between 5.5 and 30 S m^{-1} for $\sigma_s = -0.1$ to -0.5, which is also in reasonably good agreement with experimental values of about 6 S m^{-1}. The reduction compared to the unmodified PB equation was by a factor of between 2 and 3.

The explicit field dependent permittivity modification yielded a profile of the permittivity not unlike those seen in microscopic simulations. The value of the permittivity near the wall was found to be lower than predicted from literature. The proton distribution of the pore exhibited saturation effects near the wall, resembling those seen in distributions with a Stern layer included. The source of this saturation, however, seemed to be the significantly lower permittivity near the wall compared to the first permittivity model, combined with a larger effective size of the H_3O^+ ions in the finite-size ion model.

The modifications to the PB equation investigated in this thesis are successful in improving the results yielded by continuum equations for electroosmotic flow under non-equilibrium settings in nano-scale pores. As such, it is a modest but worthwhile contribution to a large field of research.

6.2 Outlook

There are a few unresolved issues with the models proposed in this thesis. Firstly, the question of how to model the viscosity is still unresolved. The accuracy of the model used in this thesis is uncertain, as it was based on somewhat vague MD simulation results [2]. It seems to be accepted that the viscosity near charged surfaces increases considerably, but the how and why is still unclear. It has been found to increase with increasing surface charge density [43], which the model used in this thesis does not account for. An alternative approach to the viscosity model is to use a constant viscosity, but with an adjusted value matched to MD simulations of the water velocity. Qiao and Aluru [42] achieved good results with this model everywhere except near the walls. The behavior of the viscosity in nano-scale systems seems to be non-uniform and the mathematical description is not well understood [2]. It is clear from the results, however, that the water drag coefficient and pore conductivity are both very much affected by the viscosity, underlining the need for a better model.

Another unanswered question is how to model the finite-size ions when studying protons in water. The properties and behavior of such solutions is not easy to incorporate into a mean-field model and their nature is much more complex than solutions with other types of ions. The protons are shared among the water molecules available and can appear in water complexes larger than the simple H_3O^+ ion assumed in the model used in this thesis. The formation and dissolution of such water complexes happens fast [15]. The question is if this is at all possible to accurately model in a mean-field approach.

The field dependent model for the permittivity shows promise in the search for a self-consistent model. The issues regarding the finite-size ions and water concentration needs further investigation, however. Some care might have to be taken with the other system parameters as well. The fact that it seemingly under-predicts the value of the permittivity near the wall might indicate that there are more effects that need to be considered to achieve an accurate model. Including a non-zero dipole moment for the hydronium, for example, will yield larger values for the permittivity near the wall.

Ultimately, a main goal would be to build a pore network model, representing a macroscopic PEM. Such a model should be based on the dynamics of individual nano-pores, as exhibited in this thesis. This approach would then yield water drag and conductivity values as measured experimentally.

Bibliography

[1] A.J. Bard and L.R. Faulkner. *Electrochemical methods: fundamentals and applications*. Wiley, 2000.

[2] M.Z. Bazant, M.S. Kilic, B.D. Storey, and A. Ajdari. Towards an understanding of induced-charge electrokinetics at large applied voltages in concentrated solutions. *Advances in Colloid and Interface Science*, 152(1–2):48 – 88, 2009.

[3] P. Berg and J. Findlay. Analytical solution of the Poisson-Nernst-Planck-Stokes equations in a cylindrical channel. *Proc. R. Soc A*, 467:3157, 2009.

[4] P. Berg and K. Lapido. Exact solution of an electro-osmotic flow problem in a cylindrical channel of polymer electrolyte membranes. *Proc. R. Soc A*, 467:3157, 2009.

[5] P Berg, K. Promislow, J.St. Pierre, J. Stumper, and B. Wetton. Water management in PEM fuel cells. *Journal of The Electrochemical Society*, 151(3):A341–A353, 2004.

[6] J.J. Bikerman. Structure and capacity of electrical double layer. *Philosophical Magazine Series 7*, 33(220):384–397, 1942.

[7] J.O'M. Bockris and A.K.N. Reddy. *Modern electrochemistry, Volume 1*. Kluwer Academic, second edition, 1998.

[8] K. Bohinc, A. Iglic, T. Slivnik, and V. Kralj-Iglic. Free energy of electric double layer. Effect of ion size. *Elektrotehniski vestnik*, 68(4):231–235, 2001.

[9] F. Booth. The dielectric constant of water and the saturation effect. *The Journal of Chemical Physics*, 19(10):1327–1328, 1951.

[10] I Borukhov, D. Andelman, and H. Orland. Steric effects in electrolytes: A modified Poisson-Boltzmann equation. *Phys. Rev. Lett.*, 79:435–438, Jul 1997.

[11] I. Borukhov, D. Andelman, and H. Orland. Adsorption of large ions from an electrolyte solution: a modified Poisson–Boltzmann equation. *Electrochimica Acta*, 46(2–3):221 – 229, 2000.

[12] R. Devanathan. Recent developments in proton exchange membranes for fuel cells. *Energy Environ. Sci.*, 1(1):101–119, 2008.

[13] M. Eigen and E. Wicke. The thermodynamics of electrolytes at higher concentration. *The Journal of Physical Chemistry*, 58(9):702–714, 1954.

[14] M. Eikerling, Y.I. Kharkats, A.A. Kornyshev, and Y.M. Volfkovich. Phenomenological theory of electro-osmotic effect and water management in polymer electrolyte proton-conducting membranes. *Journal of the Electrochemical Society*, 145(8):2684–2699, 1998.

[15] M. Eikerling, A.A. Kornyshev, A.M. Kuznetsov, J. Ulstrup, and S. Walbran. Mechanisms of proton conductance in polymer electrolyte membranes. *The Journal of Physical Chemistry B*, 105(17):3646–3662, 2001.

[16] M.H. Eikerling and P. Berg. Poroelectroelastic theory of water sorption and swelling in polymer electrolyte membranes. *Soft Matter*, 7(13):5976–5990, 2011.

[17] A. Fick. Ueber diffusion. *Annalen der Physik*, 170(1):59–86, 1855.

[18] J.B. Freund. Electro-osmosis in a nanometer-scale channel studied by atomistic simulation. *The Journal of Chemical Physics*, 116(5):2194–2200, 2002.

[19] T.D. Gierke and W.Y. Hsu. *The cluster—network model of ion clustering in perfluorosulfonated membranes*, chapter 14, pages 283–307. American Chemical Society, 1982.

[20] T.D. Gierke, G.E. Munn, and F.C. Wilson. The morphology in Nafion perfluorinated membrane products, as determined by wide- and small-angle X-ray studies. *Journal of Polymer Science: Polymer Physics Edition*, 19(11):1687–1704, 1981.

[21] E. Gongadze, U. Van Rienen, and A. Iglič. Generalized Stern models of the electric double layer considering the spatial variation of permittvity and finite size of ions in saturation regime. *Cellular & molecular biology letters*, 16(4):576–594, 2011.

[22] E. Gongadze, U. van Rienen, V. Kralj-Iglič, and A. Iglič. Langevin Poisson-Boltzmann equation: point-like ions and water dipoles near a charged surface. *General Physiology and Biophysics*, 30(2):130, 2011.

[23] C. Heitner-Wirguin. Recent advances in perfluorinated ionomer membranes: structure, properties and applications. *Journal of Membrane Science*, 120(1):1 – 33, 1996.

[24] W.Y. Hsu and T.D. Gierke. Ion transport and clustering in Nafion perfluorinated membranes. *Journal of Membrane Science*, 13(3):307 – 326, 1983.

[25] G. Karniadakis, A. Beskok, and N. Aluru. *Microflows and nanoflows: fundamentals and simulation*. Springer, 2005.

[26] J.G. Kirkwood. The dielectric polarization of polar liquids. *The Journal of Chemical Physics*, 7(10):911–919, 1939.

[27] K.D. Kreuer, S.J. Paddison, E. Spohr, M. Schuster, and others. Transport in proton conductors for fuel-cell applications: simulations, elementary reactions, and phenomenology. *Chemical Reviews-Columbus*, 104(10):4637–4678, 2004.

[28] K.O. Ladipo, P. Berg, S.-J. Kimmerle, and A. Novruzi. Effects of radially dependent parameters on proton transport in polymer electrolyte membrane nanopores. *The Journal of Chemical Physics*, 134(7):074103, 2011.

[29] J. Larmine and A. Dicks. *Fuel cell systems explained*. John Wiley and Sons Ltd, second edition, 2003.

[30] K.R. Mauritz and R.B. Moore. State of understanding of Nafion. *Chem. Rev*, 104:4535–4585, 2004.

[31] W. Nernst. Zur Kinetik der in Lösung befindlichen Körper. *Z. Physik. Chem.*, 2:613, 1888.

[32] W. Nernst. Die elektromotorische Wirksamkeit der Jonen. *Z. Physik. Chem.*, 4:128, 1889.

[33] L. Onsager. Electric moments of molecules in liquids. *Journal of the American Chemical Society*, 58(8):1486–1493, 1936.

[34] S.J. Paddison, G. Bender, K.D. Kreuer, N. Nicoloso, and T.A. Zawodzinski. The microwave region of the dielectric spectrum of hydrated Nafion and other sulfonated membranes. *Journal of New Materials for Electrochemical Systems*, 3(4):291–300, 2000.

[35] S.J. Paddison, D.W. Reagor, and T.A. Zawodzinski Jr. High frequency dielectric studies of hydrated Nafion®. *Journal of Electroanalytical Chemistry*, 459(1):91 – 97, 1998.

[36] R. Paul and S.J. Paddison. A statistical mechanical model for the calculation of the permittivity of water in hydrated polymer electrolyte membrane pores. *The Journal of Chemical Physics*, 115(16):7762–7771, 2001.

[37] R. Paul and S.J Paddison. The phenomena of dielectric saturation in the water domains of polymer electrolyte membranes. *Solid State Ionics*, 168(3):245–248, 2004.

[38] M. Planck. Über die Erregung von Electricität und Wärme in Electrolyten. *Annalen der Physik*, 275:161–186, 1890.

[39] K.B. Prater. Polymer electrolyte fuel cells: a review of recent developments. *Journal of Power Sources*, 51(1–2):129 – 144, 1994.

[40] W.H. Press, S.A. Teukolsky, W.T. Vetterling, and B.P. Flannery. *Numerical recipes*. Cambridge University Press, third edition, 2007.

[41] R.F. Probstein. *Physicochemical hydrodynamics: an introduction*. Wiley-Interscience publication. Wiley, 2005.

[42] R. Qiao and N.R. Aluru. Multiscale simulation of electroosmotic transport using embedding techniques. *International Journal for Multiscale Computational Engineering*, 2(2):173–188, 2004.

[43] R. Qiao and N.R. Aluru. Scaling of electrokinetic transport in nanometer channels. *Langmuir*, 21(19):8972–8977, 2005.

[44] I. Rubinstein. *Electro-diffusion of ions*. Society for Industrial and Applied Mathematics, 1990.

[45] I. Rubinstein and B. Zaltzman. Electro-osmotically induced convection at a permselective membrane. *Phys. Rev. E*, 62:2238–2251, Aug 2000.

[46] K. Schmidt-Rohr and Q. Chen. Parallel cylindrical water nanochannels in Nafion fuel-cell membranes. *Nature Materials*, 7:75 – 83, 2008.

[47] B. Smitha, S. Sridhar, and A.A. Khan. Solid polymer electrolyte membranes for fuel cell applications—a review. *Journal of Membrane Science*, 259(1–2):10 – 26, 2005.

[48] A.P. Thompson. Nonequilibrium molecular dynamics simulation of electro-osmotic flow in a charged nanopore. *The Journal of Chemical Physics*, 119(14):7503–7511, 2003.

[49] S. Walbran and A.A. Kornyshev. Proton transport in polarizable water. *The Journal of Chemical Physics*, 114(22):10039–10048, 2001.

[50] Y. Wang, K.S. Chen, J. Mishler, S.C. Cho, and X.C. Adroher. A review of polymer electrolyte membrane fuel cells: technology, applications, and needs on fundamental research. *Applied Energy*, 88(4):981–1007, 2011.

[51] T.A. Zawodzinski, J. Davey, J. Valerio, and S. Gottesfeld. The water content dependence of electro-osmotic drag in proton-conducting polymer electrolytes. *Electrochimica Acta*, 40(3):297 – 302, 1995.